약학박사 학위논문

Pharmacokinetics of ABN401 and volitinib, specific inhibitors of c-MET receptor kinase, in preclinical animal species and the predictions in humans

특이적 **c-MET** 수용체-인산화 효소 저해제인 **ABN401**과 **volitinib**의 전임상 동물종 중 체내동태 결정 및 사람으로의 체내동태 예측 연구

2017년 8월

서울대학교 대학원
약학과 약제과학 전공
노 치 경

Abstract

Pharmacokinetics of ABN401 and volitinib, specific inhibitors of c-MET receptor kinase, in preclinical animal species and the predictions in humans

Chi-Kyoung Noh

Department of Pharmaceutical Science

College of Pharmacy

The Graduate School

Seoul National University

The objectives of this study were to determine the pharmacokinetics of ABN401, a specific inhibitor of c-MET receptor kinase, in animal species of preclinical studies and to predict the pharmacokinetics in humans. In addition, the kinetics of volitinib, a reference c-MET inhibitor for ABN401, was studied in rats and scaled to human for the comparison. The pharmacokinetic parameters for the elimination and tissue distribution of ABN401 were apparently linear in rats in the intravenous dose range of 1 to 10 mg/kg, as evidence by the lack of statistical differences in the systemic clearance (CL; 15.9 ~ 20.3 mL/min/kg) and the volume of distribution (V_{ss}; 4.03 ~ 6.42 L/kg). Assuming the rat isolated hepatocyte to be an adequate model of the hepatic metabolism for ABN401 in rats, the metabolic clearance by the liver was expected to be approximately 48% of the systemic

clearance. In addition, the fecal elimination, most likely via the biliary excretion, was found to be the secondary elimination pathway (i.e., 36% of the systemic clearance) to the hepatic metabolism. Amongst the nine major tissues tested, the important organs for ABN401 distribution (i.e., K_p greater than 20) were the spleen, liver, kidney and lung. Calculated V_{ss}, based on the K_p values for the tissues and their anatomical volumes, were close to the measured (i.e., V_{ss} = MRT x CL) value, suggesting ABN401 is primarily distributed to those nine tissues. Accordingly, a PBPK model, involving perfusion rate limited distribution to the 9 tissues and linear CL from the venous circulation, was constructed for rats. The calculated plasma concentration-time profile of ABN401 by the kinetic model assuming intravenous dose range of 1 to 10 mg/kg adequately predicted the observation (i.e., AUC ratio of 0.9 ~ 1.1) in rats. To predict human pharmacokinetics of ABN401, the allometric relationship for V_{ss} and CL was constructed using the kinetic parameters obtained from four preclinical animal species (i.e., the mouse, rat, monkey and dog) and used to predict the parameter values in humans. In particular, K_p for the nine major tissues in humans were calculated from $K_{p,u}$ of the rat, and estimated $f_{u,p}$ for human with the allometric relationship. For the case of CL estimation in humans, however, the allometric scaling predicted the unexpectedly high systemic clearance for the inhibitor. Therefore, the CL equivalent to the hepatic blood flow, as a lower reference of CL for ABN401, was also considered in subsequent calculations. The PBPK modeling and allometric scaling were also carried out for volitinib, using similar kinetic techniques. When the concentration of lung, i.e., the pharmacological target tissue, was estimated by the model assuming the oral dose of 5 mg/kg, the duration

of the concentration exceeding the tentatively effective concentration (TEC, i.e., the IC_{50} divided by the free fraction of the inhibitor in the lung) was approximately 4 to 15 hours, depending on CL, while the duration was over 24 hours for the case of volitinib. Therefore, the pharmacokinetic rationale of this study for estimating of tissue distribution and in vivo PBPK model may be practically useful in predicting and interpreting pre-clinical/clinical pharmacokinetics of these two c-MET inhibitors.

Keywords: ABN401; Volitinib; c-MET inhibitor; Preclinical pharmacokinetic study; Allometric scaling; Physiologically-based pharmacokinetics; .

Student Number: 2011-30504

Contents

List of Tables

List of Figures

1. Introduction

1.1. C-MET inhibitor

It is now becoming increasingly clear that the mesenchymal-epithelial transition factor (c-MET) receptor tyrosine kinase may be involved in a number of key functions of the cell [e.g., cell proliferation, migration, invasion and angiogenesis] [1, 2]: The kinase triggers hepatocyte growth factor (HGF)-MET signaling, most likely by the phosphorylation of the tyrosine kinase, to control crucial downstream pathways [3] and, thus, the cell homeostasis [4]. While the role of the tyrosine kinase in maintaining cellular homeostasis is apparently important, the literature information clearly indicates that the enzyme may also be involved in cancer biology [5]. Abnormal expressions of c-MET kinase were noted in a number of cancerous biopsy samples collected from the lung, breast, ovary, kidney, colon, thyroid, liver, and intestine, indicating that the inhibition of this kinase could be a common therapeutic goal for a variety of anticancer therapies [6]. Consistent with this, abnormal activation of c-MET was found in up to 30% of the patients with advanced lung cancer. [7-9]

Furthermore, the inhibition of the kinase could be an important factor in overcoming the resistance acquired from other anticancer therapies (e.g. gefitinib), since the activation of the kinase may be one of the mechanisms for the gefitinib related resistance [9]. In fact, gefitinib is the first-line treatment for the advanced non-small cell lung cancer [10, 11]. To overcome the resistance to gefitinib, significant efforts have been continued to develop selective inhibitor(s) of c-MET kinase. Crizotinib, an anticancer agent recently approved for the treatment of lung cancer

with anaplastic lymphoma kinase (ALK) mutation, was originally developed as a c-MET inhibitor with an IC_{50} of 11 nM [12]. However, it was found that the drug possessed inhibitory effects to other tyrosine kinases, such as ALK, c-ros oncogene (ROS) and Recepteur d'Origine Nantais (RON), in addition to c-MET. Therefore, further experimental validation(s) may be necessary for overcoming the gefitinib resistance by the use of crizotinib. In relation to this, it was found that kidney damage could be one of the critical toxicities for specific inhibitors of c-MET as evidenced by the terminations of JNJ-3887605 and SGX128 in early phase of clinical study [13-15]. Therefore, the selection of specific c-MET inhibitor(s) with reduced kidney toxicity may be an important consideration in the new drug discovery and development. Although the selective c-MET inhibition is still one of the developmental focuses in the field, such inhibitor is not commercially available currently.

1.2. Volitinib

Volitinib (AZD6094 or HMPL504), a selective and potent inhibitor for c-MET kinase, is currently investigated in phase II clinical studies by AstraZeneka. The compound is reported to have an improved selectivity for the kinase with low IC_{50} value (viz, IC_{50} of 5 nM) [16]. In the literature, the kinase inhibitor had tumor regression effects in patient-derived xenograft models of papillary renal cell carcinomas and gastric cancer [17, 18]. Since the compound is metabolically stable and less susceptible to the inactivation by aldehyde oxidase, and also the metabolite(s) is (are) expected to be relatively soluble in aqueous media [16], a reduced renal

toxicity is anticipated for volitinib: In previous clinical studies with investigational c-MET inhibitors such as JNJ-3887605 and SGX128, the formation of insoluble metabolites was associated with renal toxicity, probably by forming insoluble metabolites, which led to the termination of the programs. The preclinical pharmacokinetic profiles of volitinib have been reported to be adequate [19] and, as a result, this kinase inhibitor is now under phase I/II investigations for use in a number of anticancer therapies including the lung, gastric and renal cancers (ClinicalTrials.gov identifier : NCT02252913, NCT02819596).

1.3. ABN401

ABN401, developed as a specific inhibitor for c-MET, is a small molecule compound with molecular weight of 567. Although the detailed information on the pharmacology / chemistry is not available in the literature, the potency of kinase inhibition was apparently high for ABN401 (IC_{50} of 3 nM *in vitro*, personable communication with Abion Inc, a domestic pharmaceutical company responsible for the preclinical development of this compound), suggesting that this compound may be therapeutically useful. In addition, the compound was chemically designed to produce aqueously soluble metabolite(s) so that the renal toxicity might be reduced. Again, the physicochemical properties of the compound are not currently available in the literature, key physicochemical variables, such as pKa of 7.49, octanol to water partition coefficient (log P) of 2.46, and the water solubility of 8 μg/mL with gray colored, free base form of the compound, were communicated personally. At the present time, the formulation of the compound (e.g., salt form) was not decided so

that additional characterization for the physicochemical properties may probably be necessary. Preclinical efficacy study is currently ongoing using animal models of tumor xenograft: The therapeutic indications for the compound are expected be the lung and gastric cancer. Detailed pharmacokinetic information for the compound is currently unavailable.

1.4. Physiologically-based pharmacokinetic (PBPK) modeling and allometric scaling

PBPK is a mathematical modeling technique for calculating and predicting the concentration-time profile of a drug in the systemic circulation and tissues using anatomical (e.g., tissue volume) and physiological variables (e.g., the perfusion rate, intrinsic clearance) [20, 21]. As a result of this structure, it is theoretically possible to calculate concentration-time profile for any given species and/or tissue(s). The steady state tissue-to-plasma concentration ratio (K_p), one of the crucial variables necessary for generating the concentration-time profile in PBPK, can now be calculated from physicochemical variables (e.g., pK_a, the octanol-to-water partition coefficient, free fraction in the plasma, blood-to-plasma concentration ratio) [22]. Other cardinal pharmacokinetic properties such as microsomal stability [23, 24] and free fraction in the plasma [25, 26] can also be estimated *in silico*. Despite the availability of these computational techniques for generating these cardinal parameters, however, the adequacy was not fully validated for more widespread use.

PBPK model/modeling is now widely believed as a reasonable and reliable

technique in predicting the clinical outcome [e.g., prediction of drug-drug interaction]. Indeed, in relevant guidelines from the European Medicines Agency and United States Food and Drug Administration, this modeling technique was listed as one of the routine evaluation methods. As stated previously, one of the important characteristics of PBPK modeling is the fact that the prediction of human pharmacokinetics is relatively straightforward (i.e., the model primarily contains anatomical/physiological variables). For a recent review of such application, please see this recent paper [27].

In addition to PBPK modeling approach, allometric scaling, a traditional approach for estimating pharmacokinetic variables in humans, can also be used to predict the concentration-time profile. Although the allometry was not analytically solved / proved for pharmacokinetics, it is generally assumed that crucial kinetic parameters (e.g., the volume of distribution and clearance) of animals can be related to body (or organ) size (or volume / weight) with a simple nonlinear function (i.e., typically known as allometric equation) such as:

$$y = aX^b$$

where y is the physiological / pharmacokinetic parameter of interest; X, an independent variable (e.g. the body size) of the biological species; a, a proportionality coefficient dependent on the selected dimensionality; and b, the exponent.

In general, to apply this method, experimental pharmacokinetic data be obtained in several animal species (at least three species) and the variables a and b are statistically estimated using linear regression analysis with log-transformed (thus, 'linearized') data. Then, the interspecies relationship can be used to extrapolate the

pharmacokinetic parameter in humans. The extrapolated parameters may be used for the generation of pharmacokinetic profiles in humans by using compartmental modeling. However, when it was necessary to scale tissue pharmacokinetics for humans in conjunction to compartmental models, this approach may be kinetically problematic since the underlying assumption of the equivalency in the distributional clearance to the tissue of interest amongst animal species may not be valid. In contrast, PBPK assumes that the tissue distribution primarily follows tissue blood flow and volume. In addition, linear kinetics has to be demonstrated in the animal species and the dose range used for the reasonable application of this scaling technique. Furthermore, since allometric scaling is generally applied for the elimination clearance and the volume of distribution, the consistency for elimination and distribution mechanisms has to be assumed amongst the species that are subjected to the scaling. Interestingly, however, it was reported that this method could be successfully applied despite the mechanistic differences in the kinetics amongst animals / man (e.g., interspecies difference in theophylline distribution) [28]. Furthermore, numerous literature data demonstrated that the allometric scaling were generally adequate for predicting pharmacokinetic parameters in man using animal data despite the fact that nonlinear pharmacokinetics and/or species differences in the kinetics may be involved [29-31]. Therefore, the literature information indicate that allometric method can be generally used to predict the pharmacokinetics in yet to be characterized species such as human.

1.5. Objectives

As indicated in the previous sections, the pharmacokinetics of ABN401 and its comparison to volitinib, a potentially competing c-MET inhibitior, were not systematically studied in the literature. Therefore, the objectives of this study are to characterize the pharmacokinetics of ABN401 in rats, and to predict systemic / tissue pharmacokinetics of ABN401 to humans using data obtained from four preclinical animal species. In addition, the pharmacokinetics of volitinib, a reference c-MET inhibitor, in rats and humans were characterized / predicted for the comparison with ABN401. As indicated in the previous section, the prediction / comparison of concentration in tissue(s) of humans can be theoretically challenging because the equivalency of drug distribution to the tissue amongst animal species may not be valids. In this thesis, therefore, we attempted to use a 'hybrid' (i.e., in part theoretical assumption and in part experimentation) approach to achieve these objectives.

2. Materials and methods

2.1. Chemicals and reagents

ABN401 was obtained from Abion Inc. (Seoul, Korea). Volitinib (M.W. 345.36, purity ≥ 98%) was purchased from Medchem Express (Monmouth Junction, NJ, USA). Quinine, formic acid and ammonium acetate was from Sigma Aldrich. Acetonitrile was also used in this study [Fischer scientific (Waltham, MA, USA)]. Dulbecco's modified eagle's medium, fetal bovine serum, non-essential amino acid, penicillin/streptomycin and HEPES solution were supplied from Welgene (Daegu, Korea). Radiochemicals, including [^{3}H] p-aminohippuric acid, [^{3}H] estrone-3-sulfate, [^{3}H] estradiol-17β-glucuronide and [^{3}H] 1-methyl-4-phenylpyridinium, were supplied from Perkinelmer (Waltham, MA, USA).

2.2. Animals

Male Sprague–Dawley (SD) rats (7 weeks old weighing 260-300 g) and ICR mouse (male, 4 weeks old, weighing 20 ~ 25g) were supplied from Orient Bio (Sungnam, Gyeonggi-do, Korea). The animals were maintained under controlled environment (temperature 22±2°C, relative humidity 50±5%; 12-h light/dark cycle) for over 1 week with free access to food and water. Experimental protocols involving the animals used in this study were reviewed by the Seoul National University Institutional Animal Care and Use Committee according to the National Institutes of Health Publication Number 85-23 Principles of Laboratory Animal Care revised in 1985.

Male beagle dogs, 5 months old, were supplied from Marshall Beijing (Wayao village, Liucun town, Chang Ping District, Beijing, 102204, China). Male cynomolgus monkey, 4 ~ 6 years old, were supplied from Nafo Vanny (Tam Phuoc Hamlet, Bien Hoa City, Dong Nai Province, Vietnam). Experimental protocols involving these animals used in this study were also reviewed by the Institutional Animal Care and Use Committee of Korea Institute of Toxicology according to the National Institutes of Health Publication Number 85-23 Principles of Laboratory Animal Care, revised in 1985. All animals used in this study were cared for in accordance with the principles outlined in the NIH publication of "Guide for the Care and Use of Laboratory Animals".

2.3. Pharmacokinetics of ABN401 in rats

2.3.1. Analytical condition for ABN401

The HPLC system was composed of Waters e2695 module (Waters Corporation, Milford, MA, USA) consisting of a degasser, a binary pump, and a refrigerated autosampler maintained at 5°C. Samples were separated on Eclipse XDB-C18 Column (3.5 μm, 2.1 × 100 mm, Agilent Technologies, Santa Clara, CA, USA). The mobile phase A and B were composed as follows, A : acetonitrile containing 0.1% formic acid, B : 5 mM ammonium acetate buffer solution (pH 9.8) adjusted with ammonium hydroxide. The mobile phase was delivered at the flow rate of 0.3 mL/min. In this study, the chromatographic run was completed in 5 min with gradient elution programmed as follows : 0 min (A:30%, B:70%), 0.5~1 min (A:70%, B:30%), 1.5 ~ 5 min (A:30, B:70%). The injection volume was set at 5 μL.

The MS/MS system, consisting of AB SCIEX API 3200 QTRAP triple quadrupole mass spectrometer equipped with ESI source (Applied Biosystems, Foster City, CA, USA), was connected to the HPLC system. MS/MS detection was performed in the multiple reaction monitoring (MRM) mode with positive ionization. The electrospray interface conditions were set to: curtain gas 25.0 psi collision gas medium, ion spray voltage 5500 V, temperature 450°C ion source gas 1 (50 psi), ion source gas 2 (60 psi). The optimized MS parameters were : declustering potential 41.0 V, entrance potential : 7.0 V, collision energy : 25.0 V, collision cell exit potential : 6.0 V tracer ion mass change : 567.2 → 467.2 for ABN401, 325.3 → 79.1 for quinine (the internal standard, IS, for the ABN401 assay). Operating the instrument and data acquisition was controlled by analyst software (Applied Biosystems, Foster City, CA, USA) version 1.4.2

2.3.2. Sample preparation

All biological samples were de-proteinated by adding 5 volumes of acetonitrile containing 100 ng/mL of IS. Then the samples were vortexed for 5 minutes and centrifuged at 4°C with 16,100g for 5 minutes. The supernatant was transferred to the analytical vial and 5 μL of the aliquot was injected into the LC/MS/MS system.

2.3.3. Blood to plasma partitioning of ABN401

To evaluate the blood to plasma concentration ratio, the fresh bloods were collected from the abdominal aorta after anesthesia in three rats, heparinized immediately (final concentration of heparin at 20 IU/mL) and placed temporarily on

ice. In a separate experiment, the designated amount of ABN401 dissolved in acetonitrile was added to the polyethylene tube and evaporated under nitrogen gas flow. Then, the heparinized rat blood (200 μL) was added to the tubes to obtain the final concentration of 100, 250, and 500 nM, (n=3 for each concentration level): The mixture was incubated at 37°C for 60 minutes on Labquake inverting shaker (c400110, Thermo Scientific, MA, USA). After the incubation, the mixture was centrifuged at 16100 g for 5 min at 4°C, and the supernatant plasma sample was collected and prepared as described in section 2.3.2. The concentration of ABN401 in plasma sample was analyzed using LC/MS/MS system.

2.3.4. Plasma protein binding

To examine the fraction of ABN401 unbound to plasma protein, the free concentration and the bound concentration of ABN401 in rat plasma were determined using rapid equilibrium dialysis (RED) device (ThermoFisher Scientific, Waltham, MA, USA). ABN401 dissolved in acetonitrile was transferred to empty polyethylene tube: The solvent was evaporated under nitrogen gas flow, and, then, blank rat plasma was added to give the final concentration to 5 μM. The plasma sample (i.e., 200 μL) containing 5 μM of ABN401 was added to the plasma chamber of RED device, while 350 μL of BupH phosphate-buffered saline (catalog# 28372, ThermoFisher Scientific, Waltham, MA, USA) was added in the buffer chamber of RED device, which was prepared by the manufacture's protocol. Then, the device was covered with sealing tape and placed in shaking incubator at 37°C, 100 rpm for 4 hours. After finishing the incubation, samples from the two chambers (i.e., the plasma samples and PBS

samples) were collected. The plasma samples were mixed with equal volume of blank PBS and the PBS samples were mixed with equal volume of blank plasma, and the samples were deproteinated as described in section 2.3.2. Both samples were determined by the LC/MS/MS assay with 5 μL of injection volume. The ratio of ABN401/IS peak area in buffer chamber to that in plasma chamber was calculated as the free fraction of the ABN401 in the plasma.

2.3.5. In vivo pharmacokinetics of ABN401 in rats

Overnight fasted male SD rats were anesthetized for surgical procedure by intramuscular injection of tiletamine HCl / zolazepam HCl (Zoletil 50, Virbac Laboratories, Carros, France) at the dose of 12.0 mg/kg and xylazine HCl (Rompun, Bayer, Korea) at the dose of 2.80 mg/kg. Femoral artery and vein were cannulated with polyethylene tubing (PE50; Clay Adams, Parsippany, NJ, USA) filled with saline for venous cannula and heparinized (20 IU/mL) saline for arterial cannula. The rats were allowed to recover from anesthesia for 3~4 hours after the surgery.

ABN401 was dissolved clearly in a dosing solution composed with DMSO, PEG400 and DDW (5%:45%:50%, v/v/v), and administrated intravenously / orally to rats (all administration volume was set at 2 mL/kg). The compound was given to rats at the dose of 1, 2, 5 and 10 mg/kg. Blood samples (150 μL) were collected from femoral arterial cannula at 0, 0.083, 0.25, 0.5, 1, 2, 4, 6, 8, 16 (or 12) and 24 h. The plasma was separated from the blood sample by centrifugation (4°C, 16100g, 5 minutes) and stored at –20°C until analysis.

2.3.6. Recovery of ABN401 to the urine, feces, and bile in rats

Overnight fasted male SD rats, 8 weeks old, weighing approximately 270 g, were subjected to tail vein injection of ABN401 at the dose of 5 mg/kg with the volume of 2 mL/kg. The rats (n=4) were placed in the metabolic cage and allowed to access food and water ad libitum. The urine and feces samples were collected at 0-2, 2-4, 4-6, 6-8, 8-10, 10-22, 22-34 and 34-48 h after dose. The feces samples were added with 9 mL/feces(g) of distilled water and the mixture was vortexed thoroughly. Urine and feces samples were stored at –20°C until analysis.

For bile collection study, 8 weeks old male SD rats (n=3) were anesthetized by Zoletil. The bile duct and femoral vein was cannulated along with the procedure as described in section 2.3.5. After the recovery from anesthesia, ABN401 was administrated to rats at the dose of 5 mg/kg via femoral venous cannula and bile sample was collected at pre-dose (0 h), 0-1, 1-2, 2-3, 3-4, 4-5, 5-6, 6-7, 7-8 and 8-24 hr. Normal saline was supplemented via femoral venous cannula. Collected bile samples were stored at –20°C until analysis.

The fraction the ABN401 dose recovered to the urine, feces or bile was estimated by the ratio of the cumulative excretion to time infinity [i.e., the cumulative ABN401 to the last sampling time (i.e., to 48 h for the urine and feces and to 24 h for the bile) plus extrapolated amount of excretion from the last sampling time to infinity (i.e, the excretion rate divided by the terminal phase slope in the plasma concentration time profile) to the intravenous dose.

When necessary, renal/fecal/biliary clearances of ABN401 were calculated using the following equation:

$$CL_{U,\ F\ or\ B} = \frac{Excretion_{R,\ F\ or\ B}{}^{\infty}}{\mathrm{AUC}_{IV}}$$

where $Excretion_{U,\ F\ or\ B}{}^{\infty}$ represents the cumulative amount of ABN401 excretion to the urine (subscript U), feces (subscript F) or bile (subscript B) from time zero to infinity and AUC_{IV} represents the area under the plasma concentration – time curve from time zero to infinity that was previously determined in a separate experiment.

2.3.7. Metabolic stability of ABN401 in rat liver microsomes

The metabolic stability was determined for ABN401 using pooled male rat liver microsome (product #452501, BD Gentest, Woburn, MA, USA). According to the manufacturer's protocol, the reaction mixture was prepared in 100 mM potassium phosphate buffer (pH 7.4) consisting of rat liver microsome (0.5 mg protein / mL) and ABN401 (final concentration of 1 μM, containing 1% acetonitrile). After pre-incubation of the mixture at 37°C water bath for 5 minutes, the reaction was initiated by adding 12 μL of NADPH-generating system [consisted of NADPH regenerating solution A (1/20 dilution, product #451220, BD gentest, Woburn, MA, USA) and NADPH regenerating solution B (1/100 dilution, product #45120, BD gentest, Woburn, MA, USA] to the mixture (the final volume of 200 μL). The mixture was then incubated at 37°C for 30 minutes: At the time of 0, 10, 20 and 30 minutes after the initiation of the reaction, 20 μL of aliquots of the mixture were collected and transferred to fresh tubes. Then, 100 μL of ice cold acetonitrile was added to the tube and the mixture vortexed for the termination of the reaction. Samples were

centrifuged at 4°C, 16100 g for 5 minutes and the concentration of the compound in the supernatant determined by the LC/MS/MS assay.

When it was necessary to determine the intrinsic clearance for ABN401 of the rat liver from the microsomal incubation, the slope of linear regression from $\log_{10}$ (percentage remaining) versus incubation time relationships (slope = K/2.303) was estimated to first calculate $T_{1/2}$ by using the equation $T_{1/2} = 0.693/K$. The following formula was used to convert $T_{1/2}$ to the CL_{int} (in units of ml/min/kg) [32].

$$CL_{int} = \frac{0.693}{\text{in vitro } T_{1/2}} \times \frac{\text{ml incubation}}{\text{mg microsomes}} \times \frac{\text{49 mg microsomes}}{\text{gram liver}} \times \frac{\text{40 gram liver}}{\text{kg body weight}}$$

In this study, standard scaling factors were used: mg protein per gram liver: 49 [33], and gram liver per kg body weight : 40 [34]. Then, assuming the well stirred model to be a reasonable model of the hepatic clearance of ABN401, the following equation was used to calculated hepatic clearance, CL_H from the intrinsic clearance:

$$CL_H = \frac{Q_H \times f_u \times CL_{int}}{Q_H + f_u \times CL_{int}}$$

where Q_H is hepatic blood flow (72 mL/min kg rat) and f_u is the fraction unbound of ABN401 in the blood.

2.3.8. Metabolic stability of ABN401 in isolated rat hepatocytes

Rat hepatocytes were isolated according to the procedure described in Yim et. al. [35] based on the two-step collagenase perfusion method [36]. Briefly, under anesthesia, the rat liver was perfused by Ca^{2+}/Mg^{2+}-free buffer at the flow rate of 20 mL/min for 5 min, through a cannulae inserted into the portal vein. For the perfusion

buffer to exit, the inferior vena cava was dissected. The perfusion medium was replaced with a buffer composed of 50 mM $CaCl_2$, and 0.5 mg/mL collagenase (Sigma-Aldrich) at the same flow rate of 20 mL/min for 10 min. When the connective tissue in the liver was digested by collagenase, the hepatocytes were dispersed in fresh perfusion buffer, and separated from the connective tissue by filtration through a sterile 50-mesh (the size of the sieve opening of 280 μm). Rat hepatocytes were further separated by centrifugation at 50 g for 5 min as a pellet. The cells were then resuspended in Krebs-Henseleit buffer (KHB) and centrifuged again at 50 g for 5 min for washing. Hepatocytes with a viability of greater than 80%, as determined by a trypan blue staining, were used in subsequent experiments. The resulting cell pellet was resuspended in 'incubation media' (Williams' media E containing 10% (v/v) fetal bovine serum, 1% (v/v) penicillin/streptomycin, and 0.01% (v/v) ITS (i.e., 10 mg/mL insulin, 5.5 mg/mL transferrin, and 5 μg/ml selenium) premix (Sigma-Aldrich) at pH 7.4).

The suspension of hepatocyte was diluted in 'incubation media' to the concentration of 1 x 10^6 cells/mL and 0.5 mL of suspension was placed into 12 well plate. The plate was pre-warmed at 37°C for 5 – 10 minutes prior to the reactions. The reaction was initiated by adding 0.5 mL of incubation media containing 2 μM of ABN401 to the 12 well plate to make final concentration of 1 μM (0.1% DMSO). The suspension media was incubated at 37°C for 60 minutes and 20 μL of aliquots were collected at the time of 0, 15, 30, 45 and 60 minutes. Each sample was added in 100 μL of ice cold acetonitrile and vortexed shortly to terminate the reaction. Samples were vortexed for 5 minutes additionally and centrifuged at 4°C, 16100 g for 5

minutes and the concentration of the compound in the supernatant determined by the LC/MS/MS assay.

When it was necessary to determine the intrinsic clearance of ABN401 of the liver from isolated hepatocyte, the kinetic conversion, essentially identical to that in the microsomal incubation study except for some differences in the scaling factors, was used as indicated in the following equation [32].

$$CL_{int} = \frac{0.693}{\text{in vitro } T_{1/2}} \times \frac{\text{mL incubation}}{10^6 \text{ cells}} \times \frac{163 \text{ x } 10^6 \text{ cells}}{\text{gram liver}} \times \frac{40 \text{ gram liver}}{\text{kg body weight}}$$

In addition, hepatic clearance was calculated by well stirred model from the intrinsic clearance as described in the previous section.

2.3.9. Tissue distribution of ABN401

Overnight fasted male SD rats were anesthetized for surgical procedure. The femoral artery and vein were cannulated as described previously. ABN401 were given to rats intravenously at the dose of 5 mg/kg with volume of 2 mL/kg. After 4 hours of the dosing, blood sample (150 μL) was collected via femoral arterial cannula and the animal was euthanized by cervical dislocation. Then, the animal was dissected immediately, and 9 major organs (i.e., the liver, kidney, spleen, small intestine, heart, lung, muscle, adipose and brain) were collected. The excised tissue was rinsed briefly with ice cold saline, and weighed, and stored at –20°C until analysis. Before homogenation of the tissue samples, 2 mL of PBS per gram tissue were added and then, the samples were homogenized using Ultra Turrax T25 homogenizer (Janke & Kunkel, Staufen, Germany). The aliquot (50 μL) of the homogenate was de-

proteinated as described in section 2.3.2., and analyzed by the LC-MS/MS assay. When necessary, the concentration ratio between the tissue and plasma at 4 h of the administration (i.e., $K_{p,apparent}$) for each tissue was calculated by dividing the concentration of ABN401 in the tissue with the plasma concentration:

$$K_{p,apparent} = \frac{C_{Tissue,\ at\ 4hr}}{C_{plasma,\ at\ 4\ hr}}$$

2.4. Prediction of human pharmacokinetics of ABN401

2.4.1. Pharmacokinetics of ABN401 in mouse, dogs and monkeys

Overnight fasted male ICR mouse were injected via tail vein at the dose of 0.4, 2 or 10 mg/kg with the volume of 2 mL/kg. ABN401 was dissolved in the dosing solution composed of DMSO : PEG400 : DDW (=5%:45%:50%). After injection, the blood samples (100 μL) were collected from retro-orbital plexus puncture at 5, 15, 30, 90, 180 or 360 minutes (n=3 mice per time point). Samples were centrifuged at 4°C, 16100 g for 5 minutes to separate plasma, and the plasma samples were deproteinated as described in section 2.3.2. The concentration of ABN401 was determined by the LC/MS/MS assay as described in section 2.3.1.

Overall process of in vivo studies with dogs and monkeys were conducted in collaboration with Korea Institute of Toxicology. Briefly, overnight fasted dogs and monkeys were intravenously administered at the dose of 1 mg/kg: The dosing solution for ABN401 consisted of 20% PEG400 in 0.1 M acetate buffer (pH 4.0). The blood samples were collected at 0, 0.083, 0.25, 0.5, 1, 2, 4, 8 and 24 h after the intravenous dosing. Samples were centrifuged at 4°C, 16100 g for 5 minutes to separate plasma

and the concentration of ABN401 was determined by the LC/MS/MS assay.

2.4.2. Plasma protein binding of mouse, dogs and monkeys

Overall procedure for this study was essentially identical to that in section 2.3.3. Briefly, 0.8 nmole of ABN401 was dissolved in 800 µL of blank plasma from mouse, dog or monkey plasma, respectively. Then, 200 µL of the mixture was added into the sample chamber of RED device (ThermoFisher Scientific, Waltham, MA, USA), along with the addition of 350 µL of phosphate-buffered saline (PBS, catalog# 28372, ThermoFisher Scientific, Waltham, MA, USA) to the buffer chamber: The device was placed in shaking incubator at 37°C, 100 rpm for 4 hours. Samples from both chambers were collected and the concentration in both chambers were analyzed for ABN401 to determine the free fraction of the compound in the plasma.

2.4.3. Estimation of K_p for mouse, dogs and monkeys

For the determination of K_p values for each species, plasma protein binding was assumed to be a major factor in determining the variation of K_p among species, as proposed by Rodgers and Rowland [22]. Thus, the equivalency of the tissue to plasma water partition coefficient ($K_{p,u}$) amongst the species was assumed in this study. The K_p value of nine tissues obtained from rats were divided by unbound fraction ($f_{u,p}$) in rats to estimate $K_{p,u}$. Then, $K_{p,u}$ values from the rat was used to calculate the K_p for mouse, dogs and monkeys by multiplying them with $f_{u,p}$ of each species by using the following equation:

$$K_p = \frac{C_{Tissue}}{C_{plasma}} = \frac{C_{Tissue}}{C_{plasma} \times f_{u,p}} \times f_{u,p} = K_{p,u} \times f_{u,p}$$

2.4.4. Allometric scaling

In this study, allometric relationship was assumed valid for the crucial pharmacokinetic parameters of ABN401:

$$Y = aW^b$$

where Y represents the mean values of CL and V_{ss} for animal species, W is the mean body weight of each species, a is the coefficient of the intercept of the trend line, and b is the slope of the trend line.

2.4.5. PBPK modelling and simulation

PBPK modeling for the plasma and lung concentration of ABN401 was performed by SimCYP software version 16 Release 1 (Simcyp Limited, Sheffield, UK). In this model, it was assumed that tissues were connected by the circulatory system (arterial and venous side) and ABN401 was eliminated by liver only. Physiological variables, such as blood flow rate or anatomical volume of each tissues required in the PBPK calculation, were obtained from the literature [37], which is the default values in SimCYP® software [38], version 16 Release 1 (SimCYP Limited, Sheffield, UK). The input parameters for PBPK model was listed in Table 3

In this study, the pharmacokinetics of ABN401 was assumed to be adequately explained by taking 9 typical tissues into consideration, with slight modification of PBPK models described in Yim et. al. [35]. Thus, the distribution of ABN401 to the typical tissue compartment may be expressed as:

In tissue compartments:

$$V_{\mathrm{Tissue}} \cdot \frac{dC_{\mathrm{tissue}}}{dt} = Q_{\mathrm{tissue}} \cdot \left(C_{\mathrm{AB}} - \frac{C_{\mathrm{tissue}} \cdot B/P}{K_{\mathrm{p,tissue}}} \right)$$

where V_{tissue}, C_{tissue} and Q_{tissue} are the tissue volume, the drug concentration in the tissue and tissue blood flow respectively. *B/P* is the blood-to-plasma concentration ratio. In this equation, the subscript AB represent the term related to the arterial blood

In the venous blood compartment:

$$V_{\mathrm{VB}} \cdot \frac{dC_{\mathrm{VB}}}{dt} = Q_{\mathrm{Ad}} \cdot \frac{C_{\mathrm{Lu}} \cdot B/P}{K_{\mathrm{p,Ad}}} + Q_{\mathrm{Br}} \cdot \frac{C_{\mathrm{Br}} \cdot B/P}{K_{\mathrm{p,Br}}} + Q_{\mathrm{He}} \cdot \frac{C_{\mathrm{He}} \cdot B/P}{K_{\mathrm{p,He}}} + Q_{\mathrm{Ki}}$$
$$\cdot \frac{C_{\mathrm{Ki}} \cdot B/P}{K_{\mathrm{p,Ki}}} + Q_{\mathrm{Mu}} \cdot \frac{C_{\mathrm{Mu}} \cdot B/P}{K_{\mathrm{p,Mu}}} + Q_{\mathrm{Li}} \cdot \frac{C_{\mathrm{Li}} \cdot B/P}{K_{\mathrm{p,Li}}} + Q_{\mathrm{RE}} \cdot \frac{C_{\mathrm{RE}} \cdot B/P}{K_{\mathrm{p,RE}}}$$
$$- Q_{\mathrm{CO}} \cdot C_{\mathrm{VB}} + Dose\ rate$$

where the subscript represents the following, VB : venous blood, Ad : adipose, Br : brain, He : heart, Kd : kidney, Mu : muscle, Li : liver, Sp : spleen, Gu : gut, and the RE : rest of body, and CO : cardiac output. Since the kinetics of the rest of the body were negligible for the pharmacokinetics of ABN401, the $K_{\mathrm{p,RE}}$ value was arbitrarily set at 0.0001. *Dose rate* refers the dosing rate of the ABN401.

In the arterial blood compartment of ABN401 :

$$V_{\mathrm{AB}} \cdot \frac{dC_{\mathrm{AB}}}{dt} = Q_{\mathrm{CO}} \cdot \left(\frac{C_{\mathrm{Lu}} \cdot B/P}{K_{\mathrm{p,Lu}}} - C_{\mathrm{AB}} \right) - CL_{total} \cdot C_{AB}$$

where V_{AB} is the arterial blood volume; C_{AB} and C_{AP} are the drug concentration in arterial blood and plasma, respectively. In this study, although we assumed that ABN401 and volitinib were primarily cleared from the body by the liver in all species, it is mathematically possible to describe the clearance from the arterial tissue as

shown in the above equation.

In the lung compartment of ABN401:

$$V_{\mathrm{Lu}} \cdot \frac{dC_{\mathrm{Lu}}}{dt} = Q_{\mathrm{CO}} \cdot \left(C_{\mathrm{VB}} - \frac{C_{\mathrm{Lu}} \cdot B/P}{K_{\mathrm{p,Lu}}} \right)$$

where V_{Lu} is the volume of lung; C_{Lu} is the drug concentration in the lung; Q_{CO} is the cardiac output; C_{VB} is the venous blood concentration of drug; *B/P* is the blood-to-plasma concentration ratio; and $K_{\mathrm{p,Lu}}$ is the tissue-to-plasma partition coefficient of the lung.

In the liver compartment of ABN401 :

$$V_{\mathrm{Li}} \cdot \frac{dC_{\mathrm{Li}}}{dt} = \left(Q_{\mathrm{Li}} - Q_{\mathrm{Sp}} - Q_{\mathrm{Gu}}\right) \cdot C_{\mathrm{AB}} + Q_{\mathrm{Sp}} \cdot \frac{C_{\mathrm{Sp}} \cdot B/P}{K_{\mathrm{p,Sp}}} + Q_{\mathrm{Gu}} \cdot \frac{C_{\mathrm{Gu}} \cdot B/P}{K_{\mathrm{p,Gu}}} - Q_{\mathrm{Li}} \cdot \frac{C_{\mathrm{Li}} \cdot B/P}{K_{\mathrm{p,Li}}} - CL_{\mathrm{u,int}} \cdot f_{\mathrm{u,plasma}} \cdot C_{\mathrm{LI}}$$

To quantitatively define the goodness of the estimation, the term AUC ratio was defined as the area under the predicted concentration-time curve divided by the area under the observed concentration-time curve. In general, the AUC ratio within two-fold error range (i.e., 0.5 to 2) regarded the model of adequate prediction in PBPK.

2.5. Comparative pharmacokinetics of ABN401 with volitinib

2.5.1. Analytical condition of volitinib

An HPLC system [Waters e2695 module (Waters Corporation, Milford, MA, USA)], consisting of a binary pump, a degasser and a refrigerated autosampler (at 4°C), was used in this study. Analytical samples were separated on a Luna CN column (3 μm, 100 Å, 2.1 × 50 mm, Phenomenex, Torrance, CA, USA), equipped with a guard cartridge (Gemini C18 4.0 mm × 3.0 mm, Phenomenex, Torrance, CA, USA) in room temperature. The mobile phase was composed of solvent A [acetonitrile containing 0.1% (v/v) formic acid] and solvent B [10 mM ammonium formate in water], and delivered at a flow rate of 0.3 mL/min. In this study, a gradient separation [i.e., the initial condition of mobile phase consisted of 5% of solvent A and 95% of solvent B; then the portion of solvent A was increased to 70% within 0.3 min, maintained for 0.4 min, the portion of A decreased to 5% within 0.3 min, and maintained until 5 min] was used in order to have a total run time of 5 min per sample.

The mass spectrometry system was composed of an API 3200 QTRAP triple quadrupole mass spectrometer equipped with a turbo ion spray source (Applied Biosystems, Foster City, CA, USA). MS/MS detection involved multiple reaction monitoring (MRM) in the positive ionization mode. The intensive tracer ion mass for each compound was 346.1 → 145.1 and 260.0 → 116.1 for volitinib and IS, respectively. Conditions for the electrospray interface were: curtain gas, 20.0 psi; collision gas, medium; ion spray voltage, 5500 V; temperature, 450°C; ion source gas 1, 50 psi and ion source gas 2, 50 psi. The optimized voltage parameters for analytes were as follows (in the order of volitinib and IS): declustering potential (26 and 46

V), entrance potential (6 and 9.5 V), collision energy (21 and 23 V) and collision cell exit potential (12 and 16 V). Data acquisition, quantification and calculations were performed by the Analyst software version 1.4.2 (Applied Biosystems, Foster City, CA, USA).

Calibration curves of volitinib was constructed with the ratio of the peak area of the analyte to that of IS against the nominal concentration of each calibration standard. A linear regression analysis with a weighing factor of $1/x^2$ was used to obtain the best-fit equation for the calibration curve.

2.5.2. In vivo pharmacokinetics of volitinib in rats

Overall procedure of surgery, administration and sample collection was virtually identical to the description in in section 2.3.5. Rats, weighing 260 ~ 360 g, were anesthetized by an intramuscular injection of tiletamine HCl/zolazepam HCl (Zoletil 50, Virbac Laboratories, Carros, France) at a dose of 12.0 mg/kg and xylazine HCl (Rompun, Bayer Korea, Republic of Korea) at a dose of 2.80 mg/kg. The femoral artery and vein were cannulated with polyethylene tubing (PE50, Clay Adams, Parsippany, NJ, USA) filled with saline for venous cannula and heparinized (20 IU/mL) saline for arterial cannula. The rats were then allowed to recover from the anesthesia for approximately 3 h after the surgery.

Volitinib was dissolved clearly in a dosing solution (DMSO : PEG400 : DDW = 5%:45%:50%, v/v/v), and administrated intravenously to rats (all administration volume was set at 2 mL/kg) at the dose of 5 mg/kg. Blood samples (150 μL) were collected from femoral arterial cannula at the time of 0, 0.083, 0.25, 0.5, 1, 2, 4, 6, 8,

16 and 24 h. The plasma was separated from the blood sample by centrifugation (4°C, 16100g, 5 minutes) and the supernatants were stored at –20°C until the assay.

2.5.3. Tissue distribution of volitinib

To determine the extent of tissue distribution for volitinib, the procedure essentially identical to that for ABN401 was used in this study (see the section 3.3.5). Briefly, overnight fasted male SD rats were anesthetized for surgical procedure, then femoral artery and vein were cannulated. The dosing solution of volitinib were given to rats intravenously at the dose of 5 mg/kg with volume of 2 mL/kg. After 4 hours of the dosing, blood samples were collected through femoral artery, and the animal was sacrificed by cervical dislocation. After an immediate dissection, the tissue samples were collected. In this study, 9 major tissues (i.e., the liver, kidney, spleen, small intestine, heart, lung, muscle, adipose and brain) were rinsed briefly with ice cold saline, and weighed, and stored at –20°C until the assay.

Before the analysis, tissue samples were thawed and added with 2 mL of PBS per gram tissue and then, the samples were homogenized. An aliquot (50 μL) of the homogenate was de-proteinated and analyzed by the LC-MSMS assay with injection volume of 5 μL for volitinib.

2.5.4. Prediction of human pharmacokinetics of volitinib

Overall scheme of predicting pharmacokinetic profiles for volitinib in human was again similar to the description in section 2.4. Briefly, the plasma concentration – time profiles for volitinib in rats were predicted by PBPK with same model of

ABN401. Input parameters were summarized in Table 4, and the physicochemical properties or values from in vitro study were mostly referred to the literature value [37] or predicted by SimCYP simulator or Chemaxon. $K_{p,u}$ of volitinib was calculated from $K_{p,apparent}$ values obtained from rat study (Table 2). Systemic clearance of volitinib was obtained from experiment (section 2.5.2). The predicted plasma concentration profiles in rats were compared with observed profile by overlaying both in same graph. Also, the AUC ratio was calculated to estimate the goodness of fit.

$$\text{AUC ratio} = \frac{AUC_{last}\ (predicted)}{AUC_{last}\ (observed)}$$

After verifying the prediction of pharmacokinetics in rats by PBPK modeling, human profiles were predicted with human input parameter. Human systemic clearance of volitinib was calculated from allometric scaling of systemic clearance data from mouse, rats, dogs and monkeys, which the data were reported in the literature [39]. $K_{p,u}$ values for 9 tissues were obtained from rat experimental data (Table 2) and the K_p value of volitinib in human was calculated by multiplying $K_{p,u}$ and $f_{u,p,human}$. Then, the lung concentration time profiles was calculated by PBPK modeling and compared with that of ABN401.

2.6. Interaction with SLC and MDR1 transporters

To study the potential interaction of transporters on the disposition of ABN401, cellular uptake of ABN401 was studied in cells expressing major drug transporters in humans. Madin-Darby canine kidney (MDCK) II cells overexpressing human OATP1B1, OATP1B3, OAT1, OAT3, OCT2 or MDR1 were cultured in Dulbecco's

modified eagle's medium supplemented with 10% fetal bovine serum, 1% non-essential amino acid, 100 units/mL penicillin, 0.1 mg/mL streptomycin, and 10 mM HEPES in humidified incubator at 37°C under 5% CO_2 [40]. Cells were seeded at the density of 5 x 10^5 cells/well in ornithine-coated 24 well plate, and cultured for 2~3 days. At the day of experiment, the culture media was replaced with experimental media based on hank's balanced solution containing 25 mM HEPES, and 25 mM glucose (pH 7.4) after washing with Dulbecco's PBS. After 30 min of pre-incubation, the uptake experiment was initiated by replacing the transport media containing 100 μM of ABN401 (final concentration, with 1% DMSO) and 1 μM of standard substrate of each transporter pathway, [i.e., for the uptake measurement trace amount of [^{3}H] p-aminohippuric acid (100 nM; standard substrate for OAT1), [^{3}H] estrone-3-sulfate (10 nM; standard substrate for OAT3), [^{3}H] estradiol-17β-glucuronide (10 nM; standard substrates for OATP1B1 and OATP1B3), and [^{3}H] 1-methyl-4-phenylpyridinium (10 nM; standard substrate for OCT2) or [^{3}H] digoxin (10 nM; standard substrate for MDR1) was added] and the plate was incubated in 37°C water bath for 10 minutes. After incubation, the media was removed and cells were washed with 500 μL of ice cold DPBS three times and cells were lysed in 200 μL of 0.1 N NaOH for overnight. An aliquot (150 μL) of the lysate was transferred to vial and 1 mL of scintillation fluid was added. After vortex mixing and standing for 2 h, the radioactivity in the mixture was counted by liquid scintillation counter (Tri-Carb 3110 TR, PerkinElmer Life Science, Boston, Massachusetts). In addition, the protein amount was determined in an aliquot (10 μL) of the lysate by bicinchoninic acid assay.

2.7. Pharmacokinetic and statistical analysis

When moment analysis is called for, a standard non-compartmental analysis was carried out with the concentration-time data to estimate the pharmacokinetic parameters using the Winnonlin® Professional 5.0.1 software (Pharsight Corporation, Mountain View, CA, USA). In this determination, the area under the concentration in plasma-time curves from time zero to infinity ($AUC_{0\text{-infinity}}$) and the area under the respective first moment–time curves from time zero to infinity ($AUMC_{0\text{-infinity}}$) for the two drugs were calculated by the linear trapezoidal method and standard area extrapolation method. The mean residence time (MRT) was also calculated using the following equation.

$$\mathrm{MRT} = \frac{\mathrm{AUMC}_{0-\mathrm{infinity}}}{\mathrm{AUC}_{0-\mathrm{infinity}}}$$

Half-life ($T_{1/2}$) was calculated from the slope (λ) of the terminal phase in log–linear portion of the concentration time profile.

$$\mathrm{T}_{1/2} = \frac{0.693}{\lambda}$$

In this study, a standard moment analysis was applied to calculate systemic clearance (CL) and steady-state volume of distribution (V_{ss}).

$$\mathrm{CL} = \frac{\mathrm{Dose}}{\mathrm{AUC}_{0-\mathrm{infinity}}}$$

$$\mathrm{V_{ss}} = \mathrm{CL} \times \mathrm{MRT}$$

The statistical difference among different groups were compared by one-way ANOVA followed by Tukey's test, using GraphPad Prisim (version 5.01) software (GraphPad Software, San Diego, CA, USA) running on a PC. In this study, $p < 0.05$

was accepted as denoting statistically significance. Values were expressed as means ± SD.

3. Results

3.1. Conditions for ABN401 and volitinib assays and their validations

Based on the chromatographic condition described in section 2.3.1, the retention time of ABN401 was 4.2 min and the IS was 3.9 min. In addition, from the ion chromatograms of the analysis of the sample containing no analyte (i.e., blank plasma only), only IS or at the level of LLOQ, the specificity of the assay was found adequate. In this study, quinine was selected as IS when considering the similarities of log P and pKa values between the IS and ABN401. Based on five calibration runs in the range of 5 ~ 1000 ng / ml, the minimum correlation was 0.994 with weighing factor of 1 / x, suggesting the assay is linear. The precision and the accuracy of the assay was within 15% of the nominal value, except the LLOQ within 20% of the nominal value.

The retention time of volitinib was 3.4 min and the IS (i.e. propranolol) was 3.7 min. The linearity for volitinib in rat plasma samples, as estimated from five separate runs of calibration curves, was adequate, as evidenced by a correlation coefficient of at least 0.99 in the range of concentration from 2 to 1000 ng/mL. The typical equation from 5 standard curves was $y = 0.0118x – 0.00087$. The precision and the accuracy of the assay was within 15% of the nominal value, except the LLOQ within 20% of the nominal value.

3.2. Blood to plasma partitioning and plasma protein binding of ABN401

In this study, the blood to plasma concentration ratio (B/P ratio) of ABN401 in

rat was determined using the following equation:

$$\text{B/P ratio} = \frac{C_{blood}}{C_{plasma}}$$

where C_{blood} and C_{plasma} represent the concentration of ABN401 in the blood and the plasma in rats, respectively. Calculated B/P ratio at the blood concentration of 100, 250 and 500 nM were 1.12 ± 0.173, 1.09 ± 0.133 and 1.24 ± 0.255, respectively. These values were not statistically different, suggesting that the partitioning of ABN401 to the rat blood cell is mediated by linear kinetics in the concentration range studied. Therefore, the overall average (i.e., average B/P of the three concentration levels) value of 1.15 ± 0.193 was used as the B/P ratio for ABN401 in subsequent calculations. Furthermore, since the B/P ratio was not statistically different from unity, we assumed that the distribution of ABN401 to blood cells is not appreciable in rats.

In this study, the extent of ABN401 binding to rat plasma proteins was examined using RED method. The unbound fraction($f_{u,p}$) was calculated by equations as follows,

$$f_{u,p} = \frac{C_{buffer\ chamber}}{C_{plasma\ chamber}}$$

where $C_{plasma\ chamber}$ and $C_{buffer\ chamber}$ represent the concentration of ABN401 in the plasma chamber and buffer chamber in RED device, respectively. In the rat plasma, the unbound fractions of ABN401 at 5 μM was 10.5 ± 0.770%, suggesting that ABN401 binding to plasma proteins in rats is extensive. An alternative method (i.e., ultrafiltration methods) was attempted for the evaluation of the unbound fraction in plasma proteins in this study: However, because of the extensive non-specific binding of the compound to the membrane of Amicon filter (MWCO: 30k, Millipore,

Bedford, MA, USA), reliable results could not be obtained.

Using methodologies similar to that in rat plasma, $f_{u,p}$ for ABN401 was determined in plasmas from mouse, dogs and monkey. The mean value of $f_{u,p}$ for each species were ranged from 0.07 to 0.12 (Table 8), suggesting that ABN401 binding to plasma proteins is generally extensive.

3.3. Pharmacokinetics of ABN401 in rats

The plasma concentration-time profiles of ABN401 in rats after intravenous or oral administration were depicted in Figure 1. In general, the profiles, regardless of the dosage or the route, could be described by poly-exponential functions. The pharmacokinetic parameters of ABN401 were estimated by standard moment analysis, and summarized in Table 1. From intravenous administration results, the dose-normalized mean AUC_{inf} values (i.e. AUC_{inf} divided by dose) were 1.04, 0.84, 0.92 and 1.05 x 10^{-3} h/mL/kg at the dose of 1, 2, 5 and 10 mg/kg, respectively. The mean systemic clearance at each dose was ranged from 15.9 to 20.3 mL/min/kg, one third of the hepatic blood flow of rat (i.e. 55.2 mL/min/kg [37]). The mean volume of distribution was ranged from 4.03 to 6.42 L/kg, which approximately was 5.7~9.1 fold larger than total body water in rats (i.e. 0.7 L/kg)1 mg/kg, suggesting that the compound is likely to gain access to the tissue. The steady state volume of distribution, clearance and half-life were not statistically different with the dose (one-way ANOVA), suggesting that the linear pharmacokinetics is a reasonable description for ABN401 in the dose range of 1~ 10 mg/kg. Absolute oral bioavailability was ranged from 33.2 to 63.1% for ABN401 and the bioavailability was not proportional to the

dosage. The underlying mechanism for the complex absorption is not known.

The accumulated amount of ABN401 excretion to the urine to 48 h and infinite time of the administration was 11.4 ± 2.90 μg and per rat and 12.7 ± 3.78 μg per rat, suggesting that approximately 0.926% of the dose recovered to the urine in rats. As a result, the urinary clearance value was estimated to be 0.868 ± 0.258 ml/min/kg and represented a minor elimination pathway. Using similar approach, the cumulative fecal excretion up to 48 h and infinite time of the administration was 451 ± 251 μg per rat and 496 ± 259 μg per rat. As a result, 36.1% of ABN401 dose is recovery to feces in rats. The cumulative amount of ABN401 excretion to the bile to 24 h and infinite time of the administration was 260 ± 62.7 μg per rat and 285 ± 76.0 μg. Therefore, 21.9% of ABN401 dose recovered to the bile in rats. Assuming the mean systemic clearances of 18.2 mL/min/kg, calculated biliary clearance was 4.13 ± 1.10 ml/min/kg for ABN401 in rats. Therefore, the fecal excretion, rather than the urinary pathway, may be important for ABN401.

Metabolic stability of ABN401 in hepatocytes was measured to evaluate the contribution of metabolic elimination by the rat liver to the overall elimination. For the incubation with isolated rat hepatocytes, the remaining percent of ABN401 in the incubation after 60 min incubation was 65.1 ± 13.4%. Accordingly, the intrinsic clearance by hepatocyte and estimated hepatic clearance calculated by well-stirred model were 15.2 ± 6.34 μL/min/10^6cells and 8.71 ± 3.23 mL/min/kg [i.e., accounting for 48% of the systemic clearance], respectively. In microsomal incubation study, the percent of ABN401 remaining in the microsomal incubation after 30 min was 75.8 ± 4.64%. Using standard scaling factors, calculated intrinsic clearance for ABN401 by

the rat liver microsome was 40.3 ± 11.2 mL/min/kg. Again, assuming well-stirred model to be a reasonable model of hepatic clearance for the inhibitor, calculated hepatic clearance was 3.82 ± 1.10 mL/min/kg in rats [i.e., accounting for 21% of the systemic clearance (18.2 mL/min/kg)].

Based on the concentration of ABN401 in the plasma and nine major tissues at 4 hours after the administration, the apparent tissue to plasma concentration ratio ($K_{p,apparent}$) was calculated and listed in Table 3. Assuming this to be an adequate representation of the steady state K_p value, the major distribution tissue (i.e., K_p, apparent over 20) was the spleen, liver, lung and kidney. The tissue concentrations of ABN401 in the liver, kidney, spleen, small intestine, heart, lung, muscle and adipose were higher than that in the plasma except brain, suggesting that the inhibitor is readily distributed throughout the body. When the $K_{p,apparent}$ values of each tissue were multiplied by the physiological volume of the tissue (viz, V_T), the sum of V_T for the nine tissues (i.e. theoretical V_{ss}) was found to be very close to observed V_{ss} (i.e. 4.03 to 6.42 L/kg), suggesting ABN401 is primarily distributed to the nine tissues .

3.4. Pharmacokinetics of ABN401 in mouse, dogs and monkeys

The plasma concentration-time profiles of ABN401 in mouse, dogs and monkeys after intravenous administration were shown in Figure 3 and Figure 4. The pharmacokinetic parameters were calculated by standard moment analysis, and listed in TABLEs 6 and 7

The mean systemic clearance in mouse among the dose of 0.4, 2 and 10 mg/kg was 27.2 ± 0.681 mL/min/kg, and this value was approximately, one fourth of the

hepatic blood flow of mouse [37]. The mean volume of distribution was 3.67 ± 0.0919 L/kg, ant the value was approximately 5-fold larger than total body water (i.e. 0.7 L/kg [41]). In general, the elimination and distribution of ABN401 in mice were apparently comparable to those in rats.

The plasma concentration profile of dogs and monkeys were obtained in the range of the time of 0 to 8 h for dogs and 0 to 4 ~8 h for monkeys. The plasma concentration data at 8 h of two monkeys, and at 24 h of three dogs and three monkeys were under limit of quantification. The pharmacokinetic parameters were calculated by the standard moment analysis, and the systemic clearance at the dose of 1 mg/kg was 60.3 ± 24.3 mL/min/kg for dogs and 52.2 ± 15.7 mL/min/kg for monkeys. The steady state volume of distribution was 8.11 ± 5.47 for dogs, and 2.88 ± 0.822 for monkeys.

3.5. PBPK modeling of ABN401 in rat, mouse, dog and monkey

Using the PBPK model depicted in Figure 10 and constants/parameters listed in Table 4, the concentration-time profile was calculated for rats assuming intravenous and oral administration of 1, 2, 5 and 10 mg/kg. The calculated profiles were generally in good agreement with the observed profiles, except for the early times of the oral administration at the lowest and highest doses. For the case of intravenous administration, the AUC ratio was approximately from 0.9 to 1.1, indicating that the PBPK prediction was adequate. Even with some deviations in the case of oral administration, the AUC ratio was ranged from 1.4 and 1.5 at the middle dose, 1.9 at the dose of 1 mg/kg and 2.2 at the dose of 10 mg/kg, indicating nonlinear kinetics in

oral absorption process.

To extend the PBPK model to animal species other than rat, the K_p of each experimental animal was calculated from $K_{p,u}$ of the rat and $f_{u,p}$ determined in these animal species. Again, the predicted plasma concentration – time profiles of mouse, dogs and monkeys were in reasonable agreement with the observed profiles (Figure 3 and Figure 4). The AUC ratio values for the mouse, dogs and monkeys were ranged from 1.0 to 1.3, suggesting that the PBPK model and the method of predicting K_p for other animals are generally adequate.

3.6. PBPK simulation of pharmacokinetics of ABN401 in human

Since the current PBPK model and K_p estimation was reasonably predictive for animal species, the extension of the model was attempted for the case of humans. For the PBPK modeling in humans, the $f_{u,p\ human}$ and systemic clearance was estimated by allometric scaling using on the kinetic data from 4 species. For the case of the systemic clearance, the predicted CL for humans was 77.4 mL/min/kg, the value close to the human cardiac output (i.e. 78.6 mL/min/kg). In contrast, the clearance values obtained from the monkey and the dog were generally lower (i.e., close to or somewhat larger than the liver blood flow). For the case rodents, the clearance was only a fraction of their hepatic blood flow. Considering the facts that ABN401 is primarily eliminated by the liver in rats, and that the systemic clearance in the dogs / monkeys was not vastly larger than their hepatic blood flow, two representative values of CL were assigned, i.e., the values from the allometric scaling as the upper reference value, and the hepatic blood flow of humans as a lower reference value, and used in

the subsequent calculations.

For c-MET inhibitors, the minimum effective concentration in the site of action (i.e., the lung) is not known. Therefore, in this study, we reasoned that in vitro IC50 would be a reasonable reference value. However, since the therapeutic effect would be exerted in an unbound form, the unbound concentration of the inhibitors has to be estimated. Theoretically, the free fraction of ABN401 in lung may be estimated by the following equation.

$$K_{p,lung,human} = 24.1 = \frac{C_t}{C_p} = \frac{f_{u,plasma}}{f_{u,lung}} = \frac{0.114}{f_{u,lung}}$$

Therefore, the $f_{u,lung}$ may be close to 0.00473. Therefore, the effective concentration may be tentatively estimated from $f_{u,lung}$ and the IC_{50}. Based on our estimation, the tentatively effective concentration (TEC) may be set at 340 ng/mL (i.e. 600 nM) for ABN401. From the PBPK model, the total concentration of ABN401 in the lung was calculated (Figure 7) and the duration of the concentration exceeding the TEC may be estimated to be approximately 4 h (i.e., CL at upper reference) or 15 h (i.e., CL at lower reference).

3.7. Comparative pharmacokinetics of ABN401 with volitinib

The plasma concentration time profiles of volitinib in rats after IV bolus or oral administration at the dose of 5 mg/kg were shown in Figure 6. The pharmacokinetic parameters, calculated by standard moment analysis, were listed in Table 9. As kinetic comparison to ABN401 at the equal dose of 5 mg/kg, the half-life, the steady state volume of distribution and the systemic clearance of volitinib was approximately one

half, one forth and one half of that of ABN401.

The apparent tissue to plasma concentration ratio at 4 h after intravenous administration was also estimated for volitinib to model its pharmacokinetics. The $K_{p,apparent}$ values of the major distributing organs for volitinib in rats were the liver (8.35 ± 1.89), gut (4.38 ± 1.26) and the kidney (4.02 ± 0.751). In general, $K_{p,\ apparent}$ was larger for ABN401 [i.e., the spleen, (i.e. 34.9 ± 15.7), liver (i.e. 24.0 ± 7.90), lung (i.e. 22.2 ± 5.23) and kidney (i.e. 21.8 ± 5.95)].

The adequacy of PBPK model for volitinib was studied in rats (Figure 6) using methods similar to the case of ABN401. The AUC ratio in the plasma concentration profile for volitinib after the intravenous and oral administration was 0.9 and 1.2 (Table 5), indicating that the PBPK model can also be used in the prediction of volitinib pharmacokinetics.

Using the rationale of the ABN401 for the prediction to human pharmacokinetics, the tissue to plasma water partition coefficient ($K_{p,u}$) of volitinib calculated from $K_{p,apparent}$ in rats (Table 3) and the literature value for $f_{u,p}$ of 0.3 [39] were used. Again, the human clearance of volitinib was calculated from an allometric relationship using the systemic clearance values from the mouse, rat, dog and monkey in the literature.

The lung concentration profile in humans was calculated with the PBPK model, assuming an oral administration of volitinib at 5 mg/kg. TEC was also calculated in the same manner as ABN401 using the estimated $f_{u,lung}$ value of 0.18 for volitinib. The duration of the lung concentration of volitinib exceeding the TEC was over 24 hours.

3.8. Interaction with SLC and MDR1 transporters

The uptake of standard substrates for major drug transporter was measured with or without 100 μM ABN401 in MDCK cells expressing OAT1, OAT3, OATP1B3, OCT2, MDR1 and BCRP. Amongst those, the uptake of the standard substrate in cells expressing OATP1B1 and MDR1 showed a statistically significant reduction, suggesting that ABN401 interacts with the two transport pathways. However, the extent of reduction was not as large as the reference inhibitors (Figure 8).

Since ABN401 may interact with OATP1B1 and MDR1, IC_{50} values were evaluated (Figure 9). When the cellular accumulation estradiol-17β-glucuronide and digoxin was plotted against the ABN401 concentration, the concentration dependent reduction was readily apparent for the two transporters: The concentration resulting in 50% inhibition (IC_{50}) value was estimated by a nonlinear regression analysis using the following equation:

$$\mathrm{E} = E_{max} \text{ x } (1 - \frac{\mathrm{C}}{\mathrm{C} + IC_{50}})$$

The IC_{50} value of ABN401 was estimated to be 48.8 ± 14.6 μM for OATP1B1. Estimation of IC_{50} value of MDR1 was not applicable because the maximal effect was not obtained in the highest concentration of the study (i.e., the solubility maximum in the culture medium)

4. Discussion

The overall objective of this study is to compare pharmacokinetics of ABN401 and volitinib, specific inhibitors for c-MET receptor kinase, in various mammalian species and particularly in humans. While ABN401 pharmacokinetic data were collected in our laboratory, the pharmacokinetic information of volitinib, a reference c-MET inhibitor of the study, was only available in a form of a poster (citation). In fact, detailed procedures for the study were not presented in the poster. Therefore, we independently characterize the pharmacokinetics in rats as confirmatory purposes: When it was necessary to use the kinetic information for volitinib in other species (i.e., for the allometric scaling), the literature information was assumed adequate and has to be used.

From systemic pharmacokinetic study with ABN401 in rats, it was noted that the elimination and the distribution of the inhibitor were apparently mediated by linear kinetics in the intravenous dose range of 1 to 10 mg/kg. In contrast, however, the kinetics of intestinal absorption appeared to be more complex for ABN401: the AUC after the oral administration was not proportionally increased with the dosage. In particular, the absolute bioavailability of the drug was lower for the low (i.e., 1 mg/kg) and high (i.e., 10 mg/kg) doses, while the bioavailability was higher in the middle doses (i.e., 2 and 5 mg/kg). The underlying mechanism(s) was not directly studied for the absorption of ABN401. From the facts that the aqueous solubility was markedly low (i.e., ~8 μg/mL for ABN401; personal communication with ABION Inc.) and that the compound may functionally interact with human MDR1 (Figure 8

and Figure 9), it is possible to speculate that the limited solubility of the drug in the intestinal fluid and/or the limited permeability of the drug by the action of the efflux transporter may be involved in the nonlinear absorption of ABN401. However, the aqueous solubility was not sufficiently high for a complete solubilization in the rat intestine, even at the lowest dosage of the compound (i.e., 1 mg/kg) [i.e., assuming the intestinal fluid volume of ~2 mL [42], the expected concentration ABN401 at 1 mg/kg (250 μg/rat) would be over 100 μg/mL]. In addition, the transporter interaction was only studied using cells expressing human MDR1 and, thus, it is possible that the kinetics of the transport may be significantly different for the inhibitor in rat P-glycoprotein so that the compound is not subjected to the efflux transport in the relevant concentration range. The solubility in simulated intestinal fluids and the kinetics of the transport across the rat intestinal tissue in Ussing chamber are currently being studied in this laboratory.

Since liver microsomes contain CYP isozymes and the majority of drug metabolism is mediated by CYP enzymes (citation), microsomal stability was initially studied under the assumption that the CYP-mediated hepatic metabolism is the primary route of elimination for ABN401. However, based on the microsomal stability and the standard scaling technique, the estimated hepatic clearance from microsomal incubation studies accounted for only 19% of the total clearance. In contrast, assuming the isolated hepatocyte to be a reasonable model of hepatic metabolism for ABN401, the hepatic metabolism estimated from hepatocyte incubation studies accounted for approximately 48% of the total clearance. Since the involvement of glucuronidation in the metabolism is less likely for ABN401

(unpublished observation), metabolic enzyme(s) in the cytosol of the rat hepatocyte may participate in the metabolic elimination of ABN401. The metabolite elucidation, along with the metabolic stability study with the rat liver cytosol, are currently on-going for ABN401. In relation to the possibility of the metabolism by soluble enzyme(s) in the liver, some c-MET inhibitors were reported to be metabolized by aldehyde oxidase, a cytosolic enzyme, to form metabolites that were not adequately soluble in aqueous media. The formation of the insoluble metabolites have been associated with the kidney damage, which resulted in the termination of clinical trials of some investigational c-MET inhibitors. Therefore, the possibility of the involvement of aldehyde oxidase and the solubility of the metabolite be further studied / confirmed.

In addition to the metabolic clearance, it was readily apparent that a significant portion of the dose was eliminated by excretory pathway(s) in rats. Although the urinary excretion was minor for ABN401 (i.e., less than 1% of the dose) in rats, the fecal excretion of the inhibitor accounted for approximately 36% of the dose in rats. Since up to 21% of the dose excreted to the bile in rats, it is possible that the majority of the fecal excretion is mediated via the biliary route. Taken the extent of fecal/biliary elimination together with that via the metabolic elimination, the liver may be the major eliminating organ for ABN401.

The one of the primary objectives of this study was to estimate human pharmacokinetics for ABN401. Pharmacokinetic scaling to humans is typically achieved by collecting the kinetic data from animal species and applying them with an allometric relationship. However, the pharmacological target site is the lung for

the drug and, thus, the use of PBPK modeling became necessary. For our tissue distribution study, $K_{p,apparent}$ (i.e., the ratio of the concentration between the tissue and the plasma 4 h after the intravenous administration) was determined for 9 major organs such as liver, kidney, spleen, small intestine, heart, lung, muscle, adipose and brain., Our theoretical examination indicates that the difference between $K_{p,apparentr}$ and K_p is less than 15% of K_p for ABN401, combining the equations demonstrated by Chen and Gross [43] and Jeong et. al [44]. Therefore, we assumed that $K_{p,apparent}$ is a reasonable approximation to K_p for ABN401 and used as K_p in subsequent calculations. Furthermore, it was found that the calculated V_{ss} (i.e., V_p and the sum of calculated V_T for the nine major tissues) was almost identical to measured V_{ss} (i.e., mean residence time multiplied by CL), suggesting ABN401 is primarily distributed to those nine tissues. Accordingly, a PBPK model, consisting of ABN401 distribution to the 9 major organs and linear hepatic elimination, was assumed and input variables selected (TABLE?) for rats. The AUC ratio for ABN401 was approximately 0.9 ~ 1.4 in rats. In particular, the prediction of the profile was virtually identical to unity (i.e., 0.9 ~ 1.1) when the compound was assumed to be given by intravenous administration at the dose range of 1-10 mg/kg. For the case of oral administration, while the prediction was adequate for middle doses, the calculated profile was somewhat deviated from the observation at the low and high doses, probably because of inadequate solubility and/or the efflux transport in the rat intestine. Despite the visual difference between the profiles, however, the AUC ratio ranged from 1.1 to 1.4 for the inhibitor, indicating that PBPK prediction is not overly deviated from the observation even at the extreme ends of the oral doses.

Since the concentration time profile for ABN401 calculated with the PBPK model was reasonably close to that of the observation in rats, we reasoned that this model could be applied to other species, including humans. To study the possibility, ABN401 pharmacokinetics was studied in mice, dogs and monkeys, and the predictability of the model was determined. In the current PBPK model, the variables in PBPK models could be divided into two major components: The first component primarily consisted of physicochemical / in vitro biopharmaceutical variables (e.g., LIST variables) specific for ABN401 and may be generally applied to any species. The second component consisted of anatomical / pharmacokinetic variables which may be specific for each species. For some of the variables (i.e., anatomical / physiological variables) in the second category, the preset values of SimCYP simulator (i.e., anatomical / physiological variables from the literature) were used. For other variables in the second category, those (i.e., V_{ss} and CL) were experimentally determined for the use in the calculation with the model. In particular, CL was obtained by non-compartmental analysis from the plasma concentration time curve obtained after intravenous administration in the animal species. For the case of K_p determination for each species, we chose to use a hybrid (i.e., experimental determination in conjunction with theoretical estimation) approach, instead of the experimental determination of K_p for each species: In theory, K_p may be regarded as the product of $K_{p,u}$ and $f_{u,p}$: Rodgers et al [22] proposed that $K_{p,u}$ be the function of interaction of drug with many biological constituents and, thus, may reflect average value, indicative of the equivalency of $K_{p,u}$ amongst species. Consistent with this statement, Berry et al. [45] found that the prediction of human V_{ss} was reasonable if

$K_{p,u}$ was assumed such equivalency among the species. Therefore, K_p for each tissue and $f_{u,p}$ were determined for ABN401 in rats and corresponding $K_{p,u}$ values calculated. In a separate study, we experimentally determined $f_{u,p}$ for each animal species. Then, we combined $K_{p,u}$ and $f_{u,p}$ to estimate K_p of each tissue in the animal species for the use in PBPK modeling.

Based on this approach, the general applicability of the PBPK model was studied for the mouse, dog, and monkey. Again, we assumed that the AUC ratio of the predicted concentration in the plasma – time profile to the observed profile was an adequate index of goodness of estimation. PBPK model prediction of ABN401 concentration profiles for mouse, dog, and monkey model (Figure 3 and Figure 4) was generally adequate, as evidenced by the AUC ratio between 1.0 to 1.3, suggesting that our strategy for estimating K_p is valid. Accordingly, we applied the PBPK model and the strategy of estimating K_p for the prediction of pharmacokinetics in humans.

When it was necessary to estimate CL in humans, an allometric relationship of systemic CL values from four species was applied. However, the estimated value for clearance in humans was unexpectedly high (i.e., the value approaching the cardiac output of the human): In contrast, the clearance of ABN401 was 1/4 ~ 1/3 of the liver blood flow in rodents while the clearance was close to and 1.5 times of the liver blood flow in dogs and monkeys, respectively. In our studies with rats, we found that the liver was the major eliminating organ for ABN401. Therefore, we chose to include the systemic clearance of the liver blood flow for human as a lower reference value for the calculation. For the estimation of K_p in humans, the strategy, similar to those used in animals, was used. However, since experimental $f_{u,p}$ was not available for

humans, we first estimated V_{ss} for humans using V_{ss} data of the four species. Then, using the relationship of:

$$V_{SS} = f_{u,p} \sum \left(K_{p,u} \cdot V_t\right) + V_P$$

where V_t and V_p represent anatomical volume of tissue and the plasma, respectively, $f_{u,p}$ in humans could readily be estimated.

By using estimated CL and K_p for humans in conjunction with the PBPK model, the concentration-time profile of ABN401 was calculated in the plasma and the lung (i.e., the pharmacological target of the inhibitor), assuming an oral administration of 5 mg/kg. Then, the duration of the lung concentration exceeding an effective concentration could be estimated. In this study, we chose to use *in vitro* IC_{50} of ABN401 as an meaningful reference value of the estimation of the effective concentration. Since the drug is likely to exert its pharmacological action in the unbound form only, we reasoned that the tissue binding has to be corrected for the estimation of the effective concentration. Therefore, $f_{u,lung}$ of ABN401 was first estimated by $K_{p,lung}$ and $f_{u,p}$, then, IC_{50} divided by $f_{u,lung}$ was set as tentative effective concentration (TEC) for ABN401.

For the case of CL obtained from the allometric scaling, the duration of the lung concentration exceeding TEC was approximately 4 hours. In contrast, the simulation with CL at the hepatic blood flow resulted in the duration exceeding the threshold of approximately 15 hours. Similar approach was used (i.e., characterization in rats, PBPK model validation and scaling to humans) to predict the lung concentration of volitinib at the equal oral dose of 5 mg/kg. Again, by using similar method for

estimating TEC, the duration of the volitinib concentration exceeding TEC was found to be approximately 24 hours. It was, however, noteworthy that $f_{u,lung}$ was highly dependent of $f_{u,p}$, which, in turn, was highly variable amongst the literature information. Therefore, this aspect of volitinib pharmacokinetics should to be clearly defined for better predictions of the tissue pharmacokinetics and of the duration of action. Furthermore, additional kinetic examination may be necessary for the estimation of the pharmacological response-time profile. Assuming the indirect pharmacodynamics model may be applicable to the c-MET inhibitors, the effect curve would be dependent on the pharmacodynamics, in addition to pharmacokinetics. The dynamic variables such as R_o and I_{max} could be significantly different between the two inhibitors so that the pharmacodynamics metric may not be proportional to the pharmacokinetics. This aspect of pharmacokinetics has to be characterized for accurate estimation of the efficacy of the c-MET inhibitors.

5. Conclusion

In this study, the pharmacokinetics for two selective inhibitors of c-MET receptor kinase were characterized in animal and attempted to scale their kinetics to humans. It was found that the method of correcting K_p by experimentally obtained $f_{u,p}$ and $K_{p,u}$ of the rat was useful for the application in PBPK modeling. For the case of ABN401, the absolute bioavailability for ABN401 was found to be dose-dependent: At the present time, the possibility of the involvement of P-glycoprotein and/or limited solubility of the compound in the intestine cannot be ruled out.

The duration of the lung concentration above the TEC (i.e., IC_{50} / $f_{u,T}$) was expected to be approximately 4-15 h, assuming the oral administration of ABN401 at 5 mg/kg. The oral administration of volitinib at the equal dose was expected to result in in the duration above the threshold concentration of approximately 24 h, suggesting that the pharmacokinetics of ABN401 in the lung (e.g., the duration of lung concentration above IC_{50} / $f_{u,T}$) appeared less favorable to that of volitinib. However, considering the fact that the effect-time profile is also dependent on the pharmacodynamics value from the allometric scaling, in addition to pharmacokinetics, this aspect of selective c-MET inhibitors be considered before the final evaluation.

6. Tables

Table 1. Pharmacokinetic parameters of ABN401 after intravenous and oral administration at the dose of 1, 2, 5, 10 mg/kg in rats.

IV	1 mg/kg	2 mg/kg	5 mg/kg	10 mg/kg
$T_{1/2}$ (h)	6.4 ± 0.512	4.1 ± 0.11	4.6 ± 0.468	5.7 ± 0.507
AUC_{0-24} (h·μg/mL)	0.98 ± 0.321	1.63 ± 0.159	4.33 ± 0.481	10.3 ± 0.822
$AUC_{infinite}$ (h·μg/mL)	1.04 ± 0.35	1.66 ± 0.165	4.42 ± 0.509	10.5 ± 0.762
V_{ss} (L/kg)	6.42 ± 1.53	4.8 ± 0.318	5.31 ± 0.662	4.03 ± 0.997
CL (mL/min /kg)	17.6 ± 7.01	20.3 ± 1.91	19 ± 2.2	15.9 ± 1.13

PO	1 mg/kg	2 mg/kg	5 mg/kg	10 mg/kg
$T_{1/2}$ (h)	5.7 ± 0.411	5.6 ± 0.439	4.8 ± 0.836	4.5 ± 0.681
AUC_{0-24} (h·μg/mL)	0.32 ± 0.061	0.99 ± 0.149	2.38 ± 1.15	3.71 ± 0.53
$AUC_{infinite}$ (h·μg/mL)	0.35 ± 0.065	1.05 ± 0.174	2.46 ± 1.21	3.83 ± 0.527
T_{max} (h)	4.3 ± 3.51	1.5 ± 0.866	1.2 ± 0.764	3.8 ± 3.1
C_{max} (μg/mL)	0.03 ± 0.0021	0.15 ± 0.027	0.44 ± 0.253	0.44 ± 0.146
BA (%)	33.2	63.1	55.7	36.3

Data are expressed as the mean ± SD of triplicates (1, 2, 5 mg/kg) and quadruplicates (10 mg/kg)

Table 2. Tissue to plasma concentration ratio of ABN401 at 4 hour after intravenous administration at the dose of 5 mg/kg in rats.

Tissue	$K_{p,\ apparent}$	Tissue volume (mL/kg)[a)]	V_T (mL/kg)[b)]
Spleen	34.9 ± 15.7	2.4	83.8
Liver	24.0 ± 7.90	42	1007
Lung	22.2 ± 5.23	4.8	106
Kidney	21.8 ± 5.95	9.2	201
Gut	10.7 ± 3.90	44.4	473
Muscle	7.38 ± 0.69	488	3599
Heart	5.69 ± 2.04	3.2	18.2
Adipose	1.53 ± 0.67	40	61.1
Brain	0.22 ± 0.14	8	1.8
Plasma	1	41.6	41.6
Theoretical V_{ss} (mL/kg)[c)]			1110

Data are expressed as the mean ± SD of triplicates

a) adapted from literature [46]

b) $V_T = K_{p,apparent}$ x Tissue volume

c) Theoretical V_{ss} = Sum of V_T of 9 tissues

Table 3. Tissue to plasma concentration ratio of volitinib at 4 hour after intravenous administration at the dose of 5 mg/kg in rats.

Tissue	$K_{p,\ apparent}$	Tissue volume (mL/kg)[a)]	V_T (mL/kg)[b)]
Liver	8.35 ± 1.89	42	350
Gut	4.38 ± 1.26	44.4	194
Kidney	4.02 ± 0.751	9.2	37.0
Lung	1.65 ± 0.263	4.8	7.92
Heart	1.43 ± 0.395	3.2	4.58
Spleen	1.37 ± 0.438	2.4	3.29
Muscle	0.97 ± 0.190	488	473
Adipose	0.55 ± 0.122	40	22
Brain	0.10 ± 0.0151	8	0.8
Plasma	1	41.6	41.6
Theoretical V_{ss} (mL/kg)[c)]			1140

Data are expressed as the mean ± SD of triplicates

a) adapted from literature [46]

b) $V_T = K_{p,apparent}$ x Tissue volume

c) Theoretical V_{ss} = Sum of V_T of 9 tissues

Table 4. Summary of kinetic parameters for ABN401 and volitinib used in PBPK calculation.

Parameter	ABN401	Volitinib
Molecular weight (g/mol)	567	345.4
Log P	2.46 (experimental)	0.99 (ChemAxon)
Compound type	Monoprotic base	
pKa	7.49 (experimental)	6.4 (Chemaxon)
$f_{u,p}$	0.105 (rat) 0.07 (mouse) 0.12 (dog) 0.081(monkey)	0.3 (rat)
$f_{u,p}$ (human)	0.114 (calculated)	0.46 (calculated)
B/P	1.15	0.75 (predicted)
Absorption		
MDCKII permeability	12.5 x 10^6 cm/s	-
Caco-2 cell permeability	-	30 x 10^6 cm/s
Distribution		
$K_p = K_{p,u}$, x $f_{u,p}$	rat (Table 2) mouse (section 2.4.3) dog (section 2.4.3) monkey (section 2.4.3)	rat (Table 3)
Elimination		
Systemic clearance (mL/min/kg)	18.2 (rat) 27.2 (mouse) 60.3 (dog) 52.2 (monkey)	9.88 (rat)

Table 5. AUC_{last} ratio

Species / dose (mg/kg)		AUC_{last} Observed (h·μg/mL)	AUC_{last} Predicted (h·μg/mL)	AUC ratio (pred./obs.)
ABN401				
Rat				
IV	1	0.981	0.911	0.9
	2	1.63	1.82	1.1
	5	4.33	4.56	1.1
	10	10.3	9.11	0.9
PO	1	0.319	0.703	2.2
	2	0.991	1.41	1.4
	5	2.38	3.52	1.5
	10	3.71	7.03	1.9
Mouse				
0.4		0.234	0.227	1.0
2		1.05	1.13	1.1
10		5.53	5.67	1.0
Dog				
1		0.292	0.354	1.2
Monkey				
1		0.337	0.452	1.3
Volitinib				
Rat				
5 (IV)		9.18	8.45	0.9
5 (PO)		5.86	6.97	1.2

Table 6. Pharmacokinetic parameters of ABN401 in mouse after intravenous administration at 0.4, 2 and 10 mg/kg.

Dose (mg/kg)		0.4	2	10	Average
half-life	h	1.48	2.15	1.9	1.84 ± 0.046
AUC_{last}	h*μg/mL	234.4	1052	5529	-
AUC_{inf}	h*μg/mL	254.5	1184	6102	-
CL	mL/min/kg	26.2	28.2	27.3	27.2 ± 0.681
V_{ss}	L/kg	3.14	4.08	3.81	3.67 ± 0.0919

Data are expressed as the mean ± SD of triplicates

Table 7. Pharmacokinetic parameters of ABN401 in dogs and monkeys after intravenous administration at the dose of 1 mg/kg.

		Dog	Monkey
half-life	h	1.94 ± 0.69	0.878 ± 0.293
AUC_{last}	h*μg/mL	0.292 ± 0.134	0.337 ± 0.115
AUC_{inf}	h*μg/mL	0.312 ± 0.137	0.341 ± 0.113
CL	mL/min/kg	60.3 ± 24.3	52.2 ± 15.7
V_{ss}	L/kg	8.11 ± 5.47	2.88 ± 0.822

Data are expressed as the mean ± SD of triplicates

Table 8. Plasma protein bindings in mouse, rats, dogs and monkeys of ABN401

Species	f_{up}
Mouse	0.070 ± 0.005
Rat	0.105
Dog	0.120 ± 0.005
Monkey	0.081 ± 0.002

** $f_{up,human}$ (predicted) : 0.114

Table 9. Pharmacokinetic parameters of volitinib after intravenous administration in rats at the dose of 5 mg/kg

Parameters	Unit	Values
$AUC_{0\text{-}24h}$	h*μg/mL	(PO) 5.86 ± 1.37
		(IV) 9.18 ± 3.10
AUC_{inf}	h*μg/mL	(PO) 5.89 ± 1.40
		(IV) 9.21 ± 3.12
BA	%	64
T_{max}	h	1.33 ± 0.577
C_{max}	μg/mL	1.57 ± 0.527
$T_{1/2}$	h	2.35 ± 0.887
V_{ss}	L/kg	1.26 ± 0.193
CL	mL/min/kg	9.88 ± 3.30
MRT	h	2.35 ± 1.04

Data are expressed as the mean ± SD of triplicates

7. Figures

A

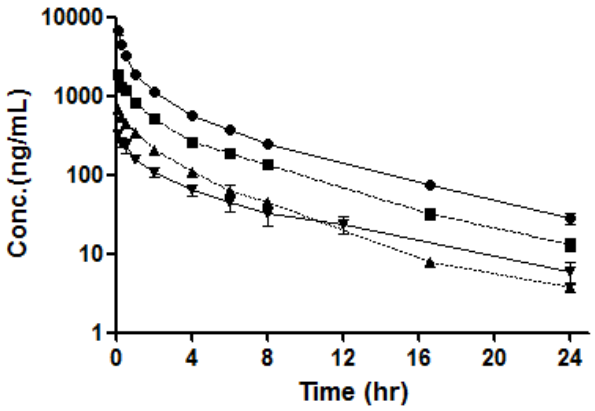

B

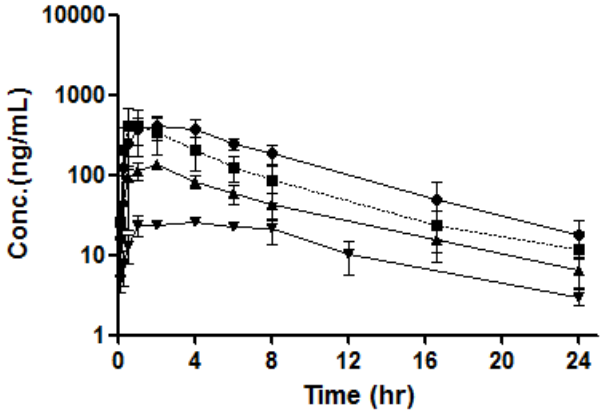

Figure 1. Temporal profiles for the plasma concentration of ABN401 after an IV bolus (A) or oral administration (B) of 1 (▼), 2 (▲), 5 (■) and 10 (●) mg/kg dose. Data are expressed as the mean ± SD of triplicates (1, 2, 5 mg/kg) and quadruplicates (10 mg/kg) runs.

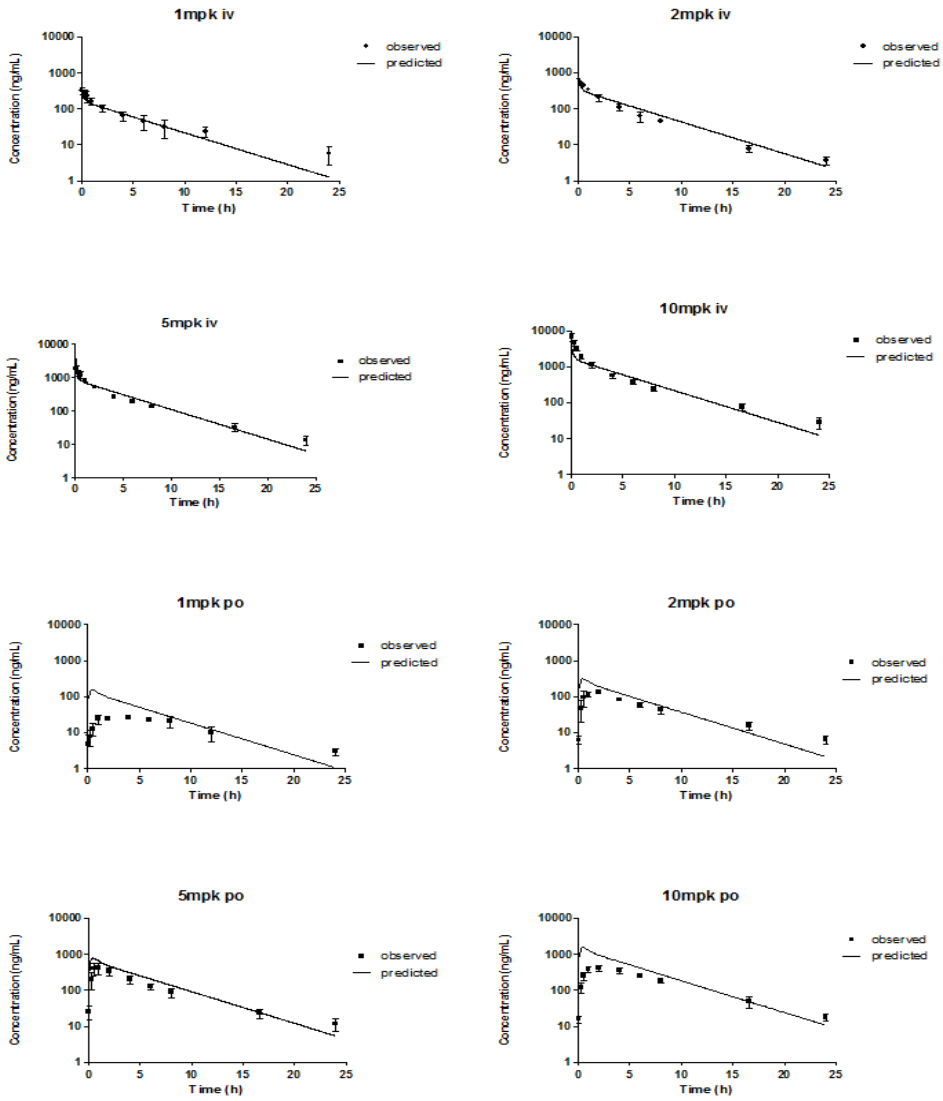

Figure 2. Observed and predicted plasma concentration–time profiles of ABN401 in rats. Black circles represent the observed concentration of ABN401 and solid line represents the predicted concentration by PBPK model using Simcyp simulator.

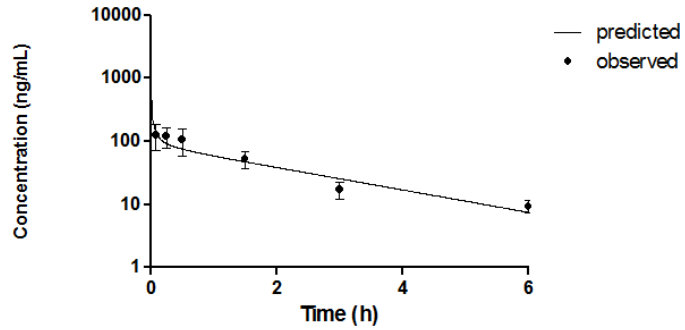

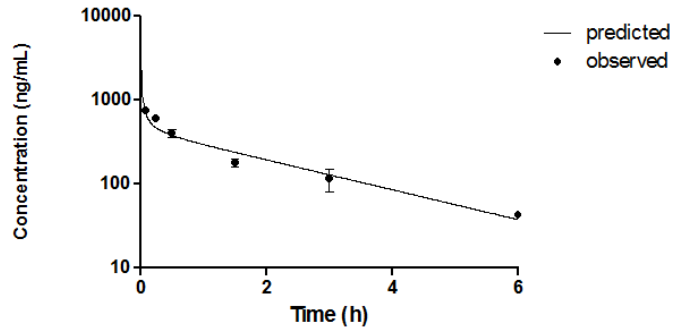

C

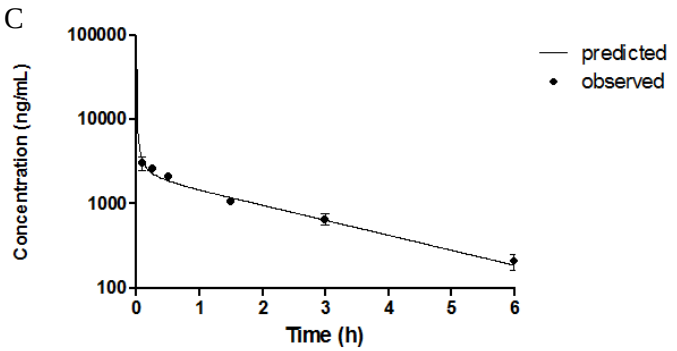

Figure 3. Observed and predicted plasma concentration–time profiles of ABN401 in mouse at the dose of 0.4 (A), 2 (B) and 10 (C) mg/kg.

A

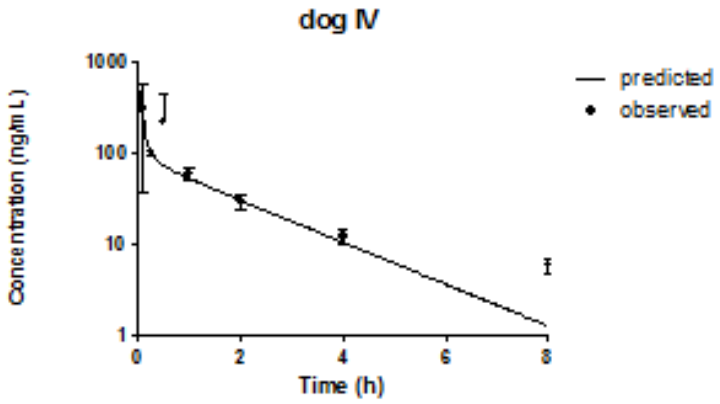

B

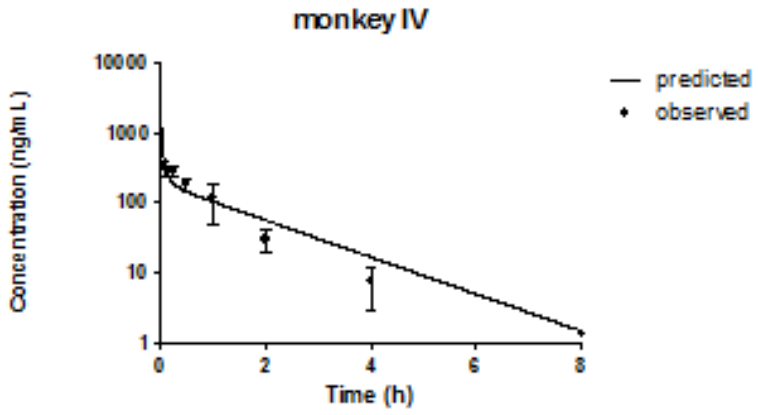

Figure 4. Observed and predicted plasma concentration–time profiles of ABN401 in dogs (A) and monkeys (B).

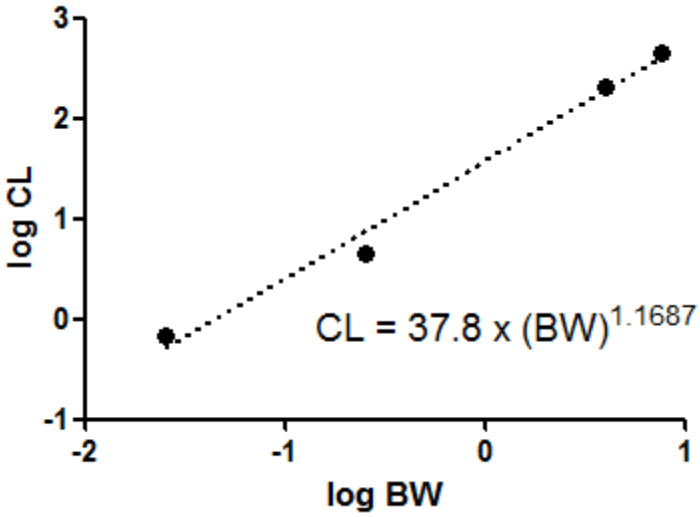

Figure 5. The log-log plot of systemic clearance of ABN401 versus body weight in mouse, rats, dogs and monkeys. The allometric equation of the systemic clearance was transformed from linear regression equation in log-log plot.

A

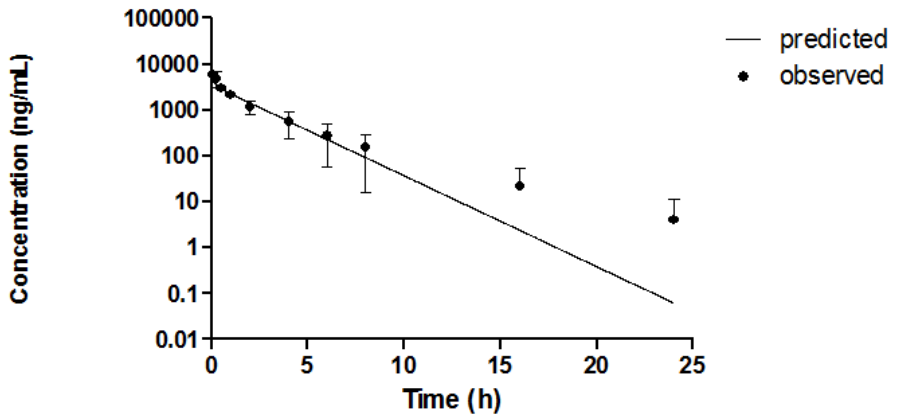

B

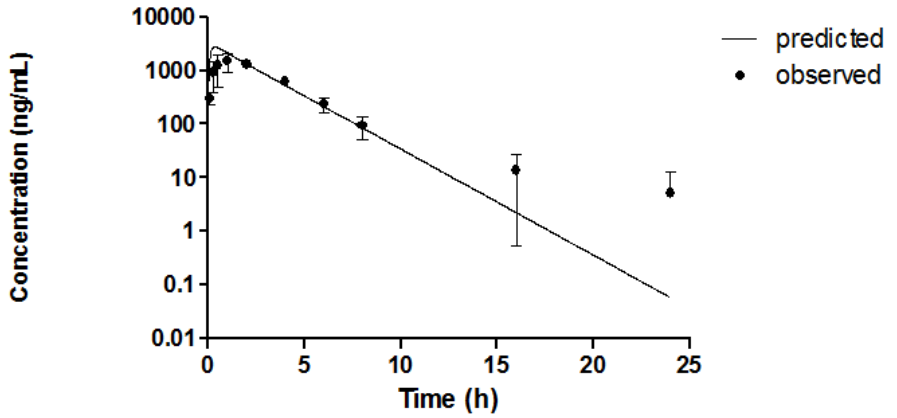

Figure 6. Observed and predicted plasma concentration–time profiles of volitinib after intravenous (A) or oral (B) administration in rats.

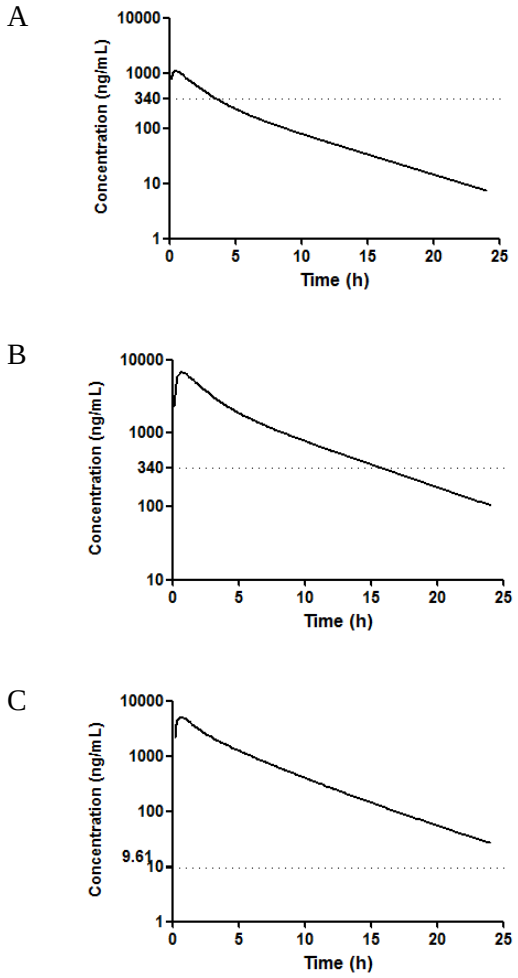

Figure 7. Predicted lung concentration – time profile of ABN401 and volitinib over 24 h in human, assuming at the dose of 5 mg/kg after oral administration: (A) when CL of ABN401 from allometric scaling, (B) when CL of ABN401 equivalent to the hepatic blood flow (C) when CL of volitinib from allometric scaling. Dashed line represents the tentative effective concentration of ABN401 or volitinib.

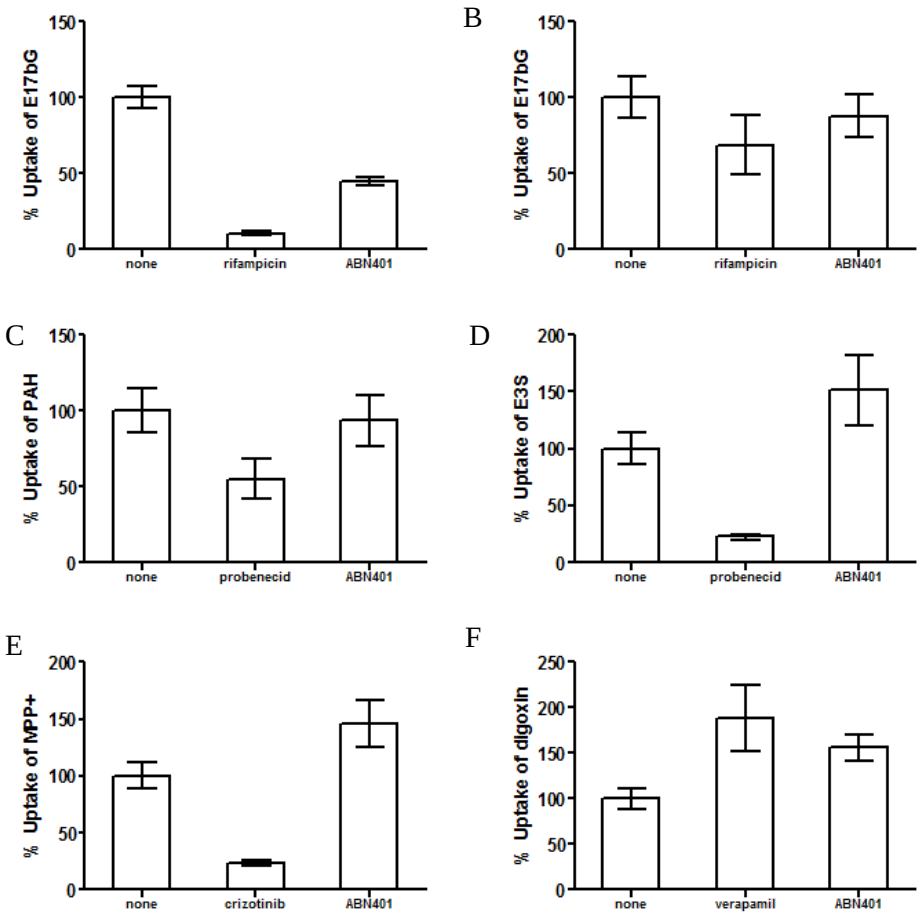

Figure 8. The uptake amount of probe substrate of (A) OATP1B1, (B) OATP1B3, (C) OAT1, (D) OAT3, (E) OCT2, and (F) MDR1 when co-incubated with 1 μM of probe substrate alone, 100 μM of reference inhibitor and ABN401, respectively.

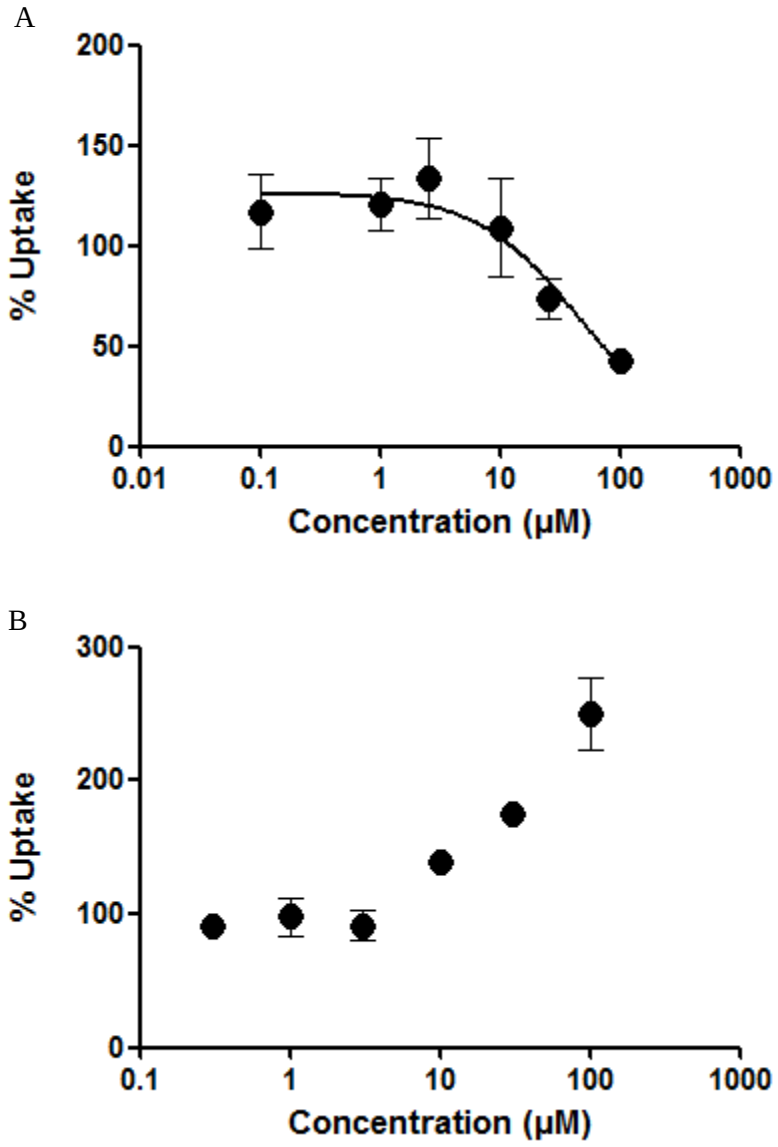

Figure 9. The uptake amount of probe substrate of (A) OATP1B1, and (B) MDR1 when co-incubated at various concentration of ABN401.

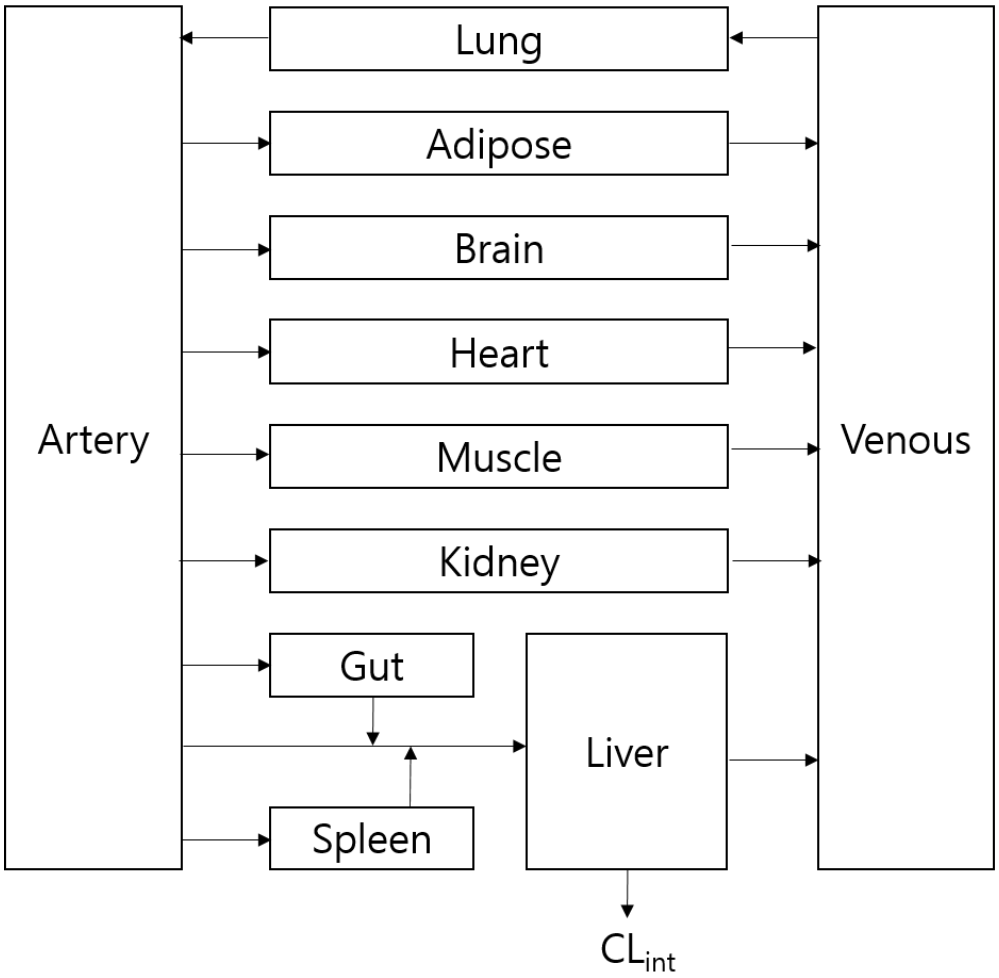

Figure 10. Schematic diagram of the PBPK model

8. Reference

1. Gherardi, E., Birchmeier, W., Birchmeier, C., and Woude, G.V., *Targeting MET in cancer: rationale and progress.* Nat. Rev. Cancer., 2012. **12**(2): p. 89-103.
2. Organ, S.L. and Tsao, M.-S., *An overview of the c-MET signaling pathway.* Ther. Adv. Med. Oncol., 2011. **3**(1 suppl): p. S7-S19.
3. Cantley, L.G. and Cantley, L.C., *Signal transduction by the hepatocyte growth factor receptor, c-met. Activation of the phosphatidylinositol 3-kinase.* J. Am. Soc. Nephrol., 1995. **5**(11): p. 1872-81.
4. Trusolino, L. and Comoglio, P.M., *Scatter-factor and semaphorin receptors: cell signalling for invasive growth.* Nat. Rev. Cancer., 2002. **2**(4): p. 289-300.
5. Bottaro, D.P., Rubin, J.S., Faletto, D.L., Chan, A.M., Kmiecik, T.E., Vande Woude, G.F., and Aaronson, S.A., *Identification of the hepatocyte growth factor receptor as the c-met proto-oncogene product.* Science, 1991. **251**(4995): p. 802-4.
6. Sierra, J.R., Tsao, M.-S., and de Bono, J.S., *c-MET as a potential therapeutic target and biomarker in cancer.* Ther. Adv. Med. Oncol., 2011. **3**(1_suppl): p. S21-S35.
7. Helena, A.Y., Arcila, M.E., Rekhtman, N., Sima, C.S., Zakowski, M.F., Pao, W., Kris, M.G., Miller, V.A., Ladanyi, M., and Riely, G.J., *Analysis of tumor specimens at the time of acquired resistance to EGFR-TKI therapy in 155 patients with EGFR-mutant lung cancers.* Clin. Cancer Res., 2013. **19**(8): p.

2240-2247.

8. Beau-Faller, M., Ruppert, A.-M., Voegeli, A.-C., Neuville, A., Meyer, N., Guerin, E., Legrain, M., Mennecier, B., Wihlm, J.-M., and Massard, G., *MET gene copy number in non-small cell lung cancer: molecular analysis in a targeted tyrosine kinase inhibitor naive cohort.* J. Thorac. Oncol., 2008. **3**(4): p. 331-339.

9. Engelman, J.A., Zejnullahu, K., Mitsudomi, T., Song, Y., Hyland, C., Park, J.O., Lindeman, N., Gale, C.-M., Zhao, X., and Christensen, J., *MET amplification leads to gefitinib resistance in lung cancer by activating ERBB3 signaling.* Science, 2007. **316**(5827): p. 1039-1043.

10. Sequist, L.V., Martins, R.G., Spigel, D., Grunberg, S.M., Spira, A., Jänne, P.A., Joshi, V.A., McCollum, D., Evans, T.L., Muzikansky, A., Kuhlmann, G.L., Han, M., Goldberg, J.S., Settleman, J., Iafrate, A.J., Engelman, J.A., Haber, D.A., Johnson, B.E., and Lynch, T.J., *First-Line Gefitinib in Patients With Advanced Non–Small-Cell Lung Cancer Harboring Somatic EGFR Mutations.* J. Clin. Oncol., 2008. **26**(15): p. 2442-2449.

11. Chan, B.A. and Hughes, B.G.M., *Targeted therapy for non-small cell lung cancer: current standards and the promise of the future.* Transl. Lung Cancer Res., 2015. **4**(1): p. 36-54.

12. Zou, H.Y., Li, Q., Lee, J.H., Arango, M.E., McDonnell, S.R., Yamazaki, S., Koudriakova, T.B., Alton, G., Cui, J.J., Kung, P.P., Nambu, M.D., Los, G., Bender, S.L., Mroczkowski, B., and Christensen, J.G., *An orally available small-molecule inhibitor of c-Met, PF-2341066, exhibits cytoreductive*

antitumor efficacy through antiproliferative and antiangiogenic mechanisms. Cancer Res., 2007. **67**(9): p. 4408-17.

13. Lolkema, M.P., Bohets, H.H., Arkenau, H.-T., Lampo, A., Barale, E., de Jonge, M.J., van Doorn, L., Hellemans, P., de Bono, J.S., and Eskens, F.A., *The c-Met tyrosine kinase inhibitor JNJ-38877605 causes renal toxicity through species-specific insoluble metabolite formation.* Clin. Cancer Res., 2015. **21**(10): p. 2297-2304.

14. Infante, J.R., Rugg, T., Gordon, M., Rooney, I., Rosen, L., Zeh, K., Liu, R., Burris, H.A., and Ramanathan, R.K., *Unexpected renal toxicity associated with SGX523, a small molecule inhibitor of MET.* Invest. New Drugs, 2013. **31**(2): p. 363-369.

15. Diamond, S., Boer, J., Maduskuie, T.P., Falahatpisheh, N., Li, Y., and Yeleswaram, S., *Species-specific metabolism of SGX523 by aldehyde oxidase and the toxicological implications.* Drug. Metab. Dispos., 2010. **38**(8): p. 1277-1285.

16. Jia, H., Dai, G., Weng, J., Zhang, Z., Wang, Q., Zhou, F., Jiao, L., Cui, Y., Ren, Y., and Fan, S., *Discovery of (S)-1-(1-(Imidazo [1, 2-a] pyridin-6-yl) ethyl)-6-(1-methyl-1 H-pyrazol-4-yl)-1 H-[1, 2, 3] triazolo [4, 5-b] pyrazine (Volitinib) as a Highly Potent and Selective Mesenchymal–Epithelial Transition Factor (c-Met) Inhibitor in Clinical Development for Treatment of Cancer.* J. Med. Chem., 2014. **57**(18): p. 7577-7589.

17. Schuller, A.G., Barry, E.R., Jones, R.D., Henry, R.E., Frigault, M.M., Beran, G., Linsenmayer, D., Hattersley, M., Smith, A., and Wilson, J., *The MET*

inhibitor AZD6094 (Savolitinib, HMPL-504) induces regression in papillary renal cell carcinoma patient–derived xenograft models. Clin. Cancer Res., 2015. **21**(12): p. 2811-2819.

18. Gavine, P.R., Ren, Y., Han, L., Lv, J., Fan, S., Zhang, W., Xu, W., Liu, Y.J., Zhang, T., and Fu, H., *Volitinib, a potent and highly selective c-Met inhibitor, effectively blocks c-Met signaling and growth in c-MET amplified gastric cancer patient-derived tumor xenograft models.* Mol. Oncol., 2015. **9**(1): p. 323-333.

19. Gu, Y., Sai, Y., Wang, J., Xia, S., Wang, G., Zhao, Y., Zhang, L., Yang, W., Dai, G., and Zhang, W., *Preclinical disposition and pharmacokinetics of volitinib, a novel selective cMet inhibitor*. 2013, AACR.

20. Jones, H.M., Gardner, I.B., and Watson, K.J., *Modelling and PBPK simulation in drug discovery.* AAPS J., 2009. **11**(1): p. 155-166.

21. Edginton, A.N., Theil, F.-P., Schmitt, W., and Willmann, S., *Whole body physiologically-based pharmacokinetic models: their use in clinical drug development.* Expert Opin. Drug Metab. Toxicol., 2008. **4**(9): p. 1143-1152.

22. Rodgers, T., Leahy, D., and Rowland, M., *Physiologically based pharmacokinetic modeling 1: Predicting the tissue distribution of moderate-to-strong bases.* J. Pharm. Sci., 2005. **94**(6): p. 1259-1276.

23. Hu, Y., Unwalla, R., Denny, R.A., Bikker, J., Di, L., and Humblet, C., *Development of QSAR models for microsomal stability: identification of good and bad structural features for rat, human and mouse microsomal stability.* J. Comput.-Aided Mol. Des., 2010. **24**(1): p. 23-35.

24. Lee, P.H., Cucurull-Sanchez, L., Lu, J., and Du, Y.J., *Development of in silico models for human liver microsomal stability.* J. Comput.-Aided Mol. Des., 2007. **21**(12): p. 665-673.

25. Zhu, X.-W., Sedykh, A., Zhu, H., Liu, S.-S., and Tropsha, A., *The use of pseudo-equilibrium constant affords improved QSAR models of human plasma protein binding.* Pharm. Res., 2013. **30**(7): p. 1790-1798.

26. Lobell, M. and Sivarajah, V., *In silico prediction of aqueous solubility, human plasma protein binding and volume of distribution of compounds from calculated pKa and AlogP98 values.* Mol. Diversity, 2003. **7**(1): p. 69-87.

27. Rowland, M., Peck, C., and Tucker, G., *Physiologically-based pharmacokinetics in drug development and regulatory science.* Annu. Rev. Pharmacol. Toxicol., 2011. **51**: p. 45-73.

28. Gaspari, F. and Bonati, M., *Interspecies metabolism and pharmacokinetic scaling of theophylline disposition.* Drug. Metab. Rev., 1990. **22**(2-3): p. 179-207.

29. Polekhina, O.V., Obraztsov, N.V., Petrunin, V.A., and Vysotskaya, T.A., *Interspecies Pharmacokinetics. 1. Allometric Scaling of Pharmacokinetic Parameters (a Review).* Pharm. Chem. J., 2014. **48**(7): p. 421-429.

30. Kagan, L., Abraham, A.K., Harrold, J.M., and Mager, D.E., *Interspecies Scaling of Receptor-Mediated Pharmacokinetics and Pharmacodynamics of Type I Interferons.* Pharm. Res., 2010. **27**(5): p. 920-932.

31. Morris, M.E., Yang, X., Gandhi, Y.A., Bhansali, S.G., and Benincosa, L.J., *Interspecies scaling: prediction of human biliary clearance and comparison*

with QSPKR. Biopharm. Drug. Dispos., 2012. **33**(1): p. 1-14.

32. Obach, R.S., *Nonspecific binding to microsomes: impact on scale-up of in vitro intrinsic clearance to hepatic clearance as assessed through examination of warfarin, imipramine, and propranolol.* Drug. Metab. Dispos., 1997. **25**(12): p. 1359-1369.

33. Smith, R., Jones, R., Ballard, P., and Griffiths, H., *Determination of microsome and hepatocyte scaling factors for in vitro/in vivo extrapolation in the rat and dog.* Xenobiotica, 2008. **38**(11): p. 1386-1398.

34. Davies, B. and Morris, T., *Physiological parameters in laboratory animals and humans.* Pharm. Res., 1993. **10**(7): p. 1093-1095.

35. Yim, C.-S., Jeong, Y.-S., Lee, S.-Y., Pyeon, W., Ryu, H.-M., Lee, J.-H., Lee, K.-R., Maeng, H.-J., and Chung, S.-J., *Specific Inhibition of the Distribution of Lobeglitazone to the Liver by Atorvastatin in Rats: Evidence for an rOATP1B2-Mediated Interaction in Hepatic Transport.* Drug. Metab. Dispos., 2017.

36. Kotani, N., Maeda, K., Watanabe, T., Hiramatsu, M., Gong, L.K., Bi, Y.A., Takezawa, T., Kusuhara, H., and Sugiyama, Y., *Culture period-dependent changes in the uptake of transporter substrates in sandwich-cultured rat and human hepatocytes.* Drug. Metab. Dispos., 2011. **39**(9): p. 1503-10.

37. Brown, R.P., Delp, M.D., Lindstedt, S.L., Rhomberg, L.R., and Beliles, R.P., *Physiological parameter values for physiologically based pharmacokinetic models.* Toxicol. Ind. Health., 1997. **13**(4): p. 407-84.

38. Jamei, M., Marciniak, S., Feng, K., Barnett, A., Tucker, G., and Rostami-

Hodjegan, A., *The Simcyp population-based ADME simulator.* Expert. Opin. Drug. Metab. Toxicol., 2009. **5**(2): p. 211-23.

39. Gu, Y., Sai, Y., Wang, J., Xia, S., Wang, G., Zhao, Y., Zhang, L., Yang, W., Dai, G., Zhang, W., Gong, Q., Tian, Z., and Su, W., *Abstract 3371: Preclinical disposition and pharmacokinetics of volitinib, a novel selective cMet inhibitor.* Cancer Res., 2013. **73**(8 Supplement): p. 3371-3371.

40. Lee, J.H., Noh, C.K., Yim, C.S., Jeong, Y.S., Ahn, S.H., Lee, W., Kim, D.D., and Chung, S.J., *Kinetics of the Absorption, Distribution, Metabolism, and Excretion of Lobeglitazone, a Novel Activator of Peroxisome Proliferator-Activated Receptor Gamma in Rats.* J. Pharm. Sci., 2015. **104**(9): p. 3049-59.

41. Davies, B. and Morris, T., *Physiological parameters in laboratory animals and humans.* Pharm. Res., 1993. **10**(7): p. 1093-5.

42. McConnell, E.L., Basit, A.W., and Murdan, S., *Measurements of rat and mouse gastrointestinal pH, fluid and lymphoid tissue, and implications for in-vivo experiments.* J. Pharm. Pharmacol., 2008. **60**(1): p. 63-70.

43. Chen, H.S.G. and Gross, J.F., *Estimation of tissue-to-plasma partition coefficients used in physiological pharmacokinetic models.* J. Pharmacokinet. Biopharm., 1979. **7**(1): p. 117-125.

44. Jeong, Y.S., Yim, C.S., Ryu, H.M., Noh, C.K., Song, Y.K., and Chung, S.J., *Estimation of the minimum permeability coefficient in rats for perfusion-limited tissue distribution in whole-body physiologically-based pharmacokinetics.* Eur. J. Pharm. Biopharm., 2017. **115**: p. 1-17.

45. Berry, L.M., Li, C., and Zhao, Z., *Species Differences in Distribution and*

Prediction of Human V_{ss} from Preclinical Data. Drug. Metab. Dispos., 2011. **39**(11): p. 2103-2116.

46. Bernareggi, A. and Rowland, M., *Physiologic modeling of cyclosporin kinetics in rat and man*. J. Pharmacokinet. Biopharm., 1991. **19**(1): p. 21-50.

국문초록

c-MET 은 수용체-타이로신인산화효소 (receptor-tyrosine kinase) 중의 하나로, 이 효소의 활성화는 폐암치료의 핵심 약물인 gefitinib 에 대한 주요 내성기전의 하나로 보고되었다. ABN401 은 c-MET 에 대하여 특이적이며 강력한 저해작용을 가지며, 전임상 신약 개발 연구가 진행 중인 물질이다. 따라서, 본 연구에서는 먼저 rat 에서 이 물질의 체내동태 및 흡수, 분포, 대사, 배설 생물약제학적 연구를 최초로 보고하고, 마우스, 원숭이, 개에서의 전임상 약물동태 결과로부터 사람으로의 약물 체내동태를 추정한 다음, 동일기전 항암제로 현재 임상 2 상 개발중인 volitinib 과의 비교체내동태 연구를 수행하였다.

먼저 rat 의 주요 약물동태 파라미터를 구하였을 때, 1 ~ 10 mg/kg 의 용량범위에서 선형 체내동태를 따르는 것으로 보였고, 이 때 반감기(t1/2)는 4.1 ~ 6.4 h, 전신 클리어런스(CL)는 15.9 ~ 20.3 ml/min/kg, 전신 분포 용적(Vss)은 4.03 ~ 6.42 L/kg 임을 알았다. 소실경로 연구에서, 간세포 대사 연구로 추정한 간 클리어런스는 전신 클리어런스의 49%, 뇨 배설 클리어런스는 전체의 1%, 변으로의 배설 클리어런스는 전체의 36%에 해당할 것으로 추정하였다. 특히 주된 소실 경로에 하나인 변으로의 배설에서 담즙 클리어런스가 차지하는 분율은 약 61% 정도일 것으로 추정하였다.

Rat의 주요 9개 장기에 대한 겉보기 조직-혈장 분배계수 (Kp)로부터 추정한 조직 분포 용적의 합은 혈장농도-시간 곡선으로부터 구한 전신 분포용적(Vss)과 유사하였다. 또한 in vitro 생물약제학적 변수, 생리학적 파라미터 및 9 개 장기 PBPK 모델을 가지고 계산한 혈장 중 농도-시간 곡선의 추이는 rat 에서의 실측치와 매우 유사하였으며, 이 9 개 장기 기반의 physiologically -based pharmacokinetic (PBPK) 모델은 동태학적으로 적절할 것이라고 사료되었다.

본 연구에서는 rat 에서의 조직-비결합혈장농도 분배계수 (Kp,u)가 사람을 포함한 여러 종간에 유사할 것이라고 가정하고, 타 동물 종의 fu,plasma 와 Kp,u 로부터 조직-혈장 분배계수를 계산하고, 이를 가지고 수행한 simulation 연구에서 마우스, 개 및 원숭이에서의 혈장농도-시간 곡선의 실측치는 계산치와 유사하였다. 이 때, fu,plasma 산출치는 타 종의 체내분포 예측에 유효함을 알았다.

마우스, 랫트, 개, 원숭이의 실측 Vss 값으로부터 allometric scaling을 통해 사람에서의 Vss 를 구하고 이 때 사람의 fu,plasma 예측값을 구한 후 Kp,u 를 이용하여 사람에서의 조직-혈장 분배계수를 계산하였다. 또한 마우스, 랫트, 개, 원숭이의 실측 전신 클리어런스 데이터로부터 allometry 관계식을 결정하고 사람에서의 전신 클리어런스 추정하였으며, 이 때의 값이 심박출량에 해당하는 매우 큰 값을 가짐을 알았다. 그런데,

rat 에서의 소실 경로는 모두 간에 국한되어 있었으며 사람에서도 이와 유사할 것이라고 가정하면, 사람의 전신 클리어런스는 사람의 간혈류 이하일 것이라고 상정할 수도 있었다. 따라서 추후에는 사람의 전신클리어런스 값은 scaling 예측치를 최대값으로, 사람의 간혈류를 최소값으로 보고 simulation 연구을 진행하였다.

이러한 추정치를 바탕으로 위 PBPK 모델에 적용하여 혈장 중 약물농도와 표적 장기인 폐에서의 ABN401 의 동태를 예측하고, 비교약물인 volitinib 에도 유사한 모델링 연구를 적용하였다. 두 약물 모두 사람에 5 mg/kg 으로 하루 한번 투여되었다고 상정하였다. 표적 장기인 폐 중 농도의 추이를 계산하였을 때, ABN401 는 약 4 ~ 15 시간 동안, volitinib 은 약 24 시간 동안 예상치료농도를 유지할 것으로 예측되었다. 따라서 본 연구에서 수립한 체내동태학 모델 및 주요 변수의 예측체계는 이 두 c-MET 저해제의 전임상 / 임상 체내동태 예측 및 해석에 실용적으로 사용할 수 있을 것으로 사료되었다.

주요어: ABN401, volitinib, 약물동태, PBPK 시뮬레이션, allometric scaling

학번: 2011-30504